


Graded damage in quasi-brittle solids

Nunziante Valoroso^{1,2}  | Claude Stolz^{1,3}

¹Institut des Sciences de la Mécanique et Applications Industrielles, UMR CNRS 9219, Université Paris Saclay, Palaiseau, France

²Dipartimento di Ingegneria, Università di Napoli Parthenope, Napoli, Italy

³Institut de recherche en Génie Civil et Mécanique, UMR CNRS 6183, Ecole Centrale de Nantes, Nantes, France

Correspondence

Nunziante Valoroso, Institut des Sciences de la Mécanique et Applications Industrielles, UMR CNRS 9219, Université Paris Saclay, 7, Boulevard Gaspard Monge, Palaiseau 91120, France.
Email: nunziante.valoroso@uniparthenope.it

Abstract

A novel approach to damage modeling for quasi-brittle solids is presented relying upon a differential inclusion that is closely related to the one of implicit gradient models. The proposed formulation naturally fits in the so-called non-local standard approach, whereby the framework of generalized standard materials is extended to include gradients of internal variables to account for the physics of the fracture phenomenon in a regularized sense, that is, via extended constitutive equations in which a length scale parameter brings to the macro level information about material microstructure. This concept is fully embodied into the present approach to quasi-brittle fracture, whereby progressive damage occurs in layers of finite thickness where the gradient of damage is bounded and a fully damaged region is understood as a fracture with no ambiguity. Key to the effective implementation of the model are the choice of two constitutive functions and the implicit tracking of regions in a state of progressive damage via Lagrange multipliers acting on internal constraints. The ideas are developed for a general Cauchy continuum and representative numerical simulations are included that demonstrate the model capabilities.

KEYWORDS

damage mechanics, fracture, generalized standard materials, gradient, Lagrange multipliers, regularization, thick level sets

1 | INTRODUCTION

In the last two decades nonlocal and gradient formulations have become increasingly popular in mechanics as regularizing techniques that allow to deal with problems suffering from mesh-sensitivity and time-stepping dependence that are induced by strain softening.

In short, the idea underlying almost all such techniques is that of using some extended constitutive equations in which information about the material microstructure is synthetically represented through a characteristic length scale parameter; for instance, in concrete this is believed to be about three times the maximum aggregate size.¹ The physical interpretation of the length parameter on a micromechanical basis is however still the object of an open debate, whereby its interpretation as a mathematical regularization parameter is preferred by many Authors.

A number of successful damage models incorporating a length scale have been provided in the literature in a nonlocal, integral formulation starting from the pioneering work of Pijaudier-Cabot and Bazant.² In the same context of continuum damage mechanics, implementations of the gradient concept have then been presented in the wake of gradient approaches initially developed within plasticity theories³⁻⁵ or as mere localization limiters.⁶⁻⁹ Models of gradient type require the

This is an open access article under the terms of the Creative Commons Attribution-NonCommercial-NoDerivs License, which permits use and distribution in any medium, provided the original work is properly cited, the use is non-commercial and no modifications or adaptations are made.

© 2022 The Authors. *International Journal for Numerical Methods in Engineering* published by John Wiley & Sons Ltd.

solution of a partial differential equation in place of the explicit evaluation of averaging operators and under suitable hypotheses they can be shown to be almost equivalent to the nonlocal integral approach.¹⁰

A complete damage state is commonly understood as the formation of a discrete crack and a link between the two descriptions of material failure can be established in different ways. In this respect, the variational theory of quasi-static fracture initially developed by Francfort and Marigo¹¹ has gained in recent years a considerable interest in the scientific community. Basically, it relies upon minimization of a functional obtained from the sum of an elastic bulk energy and a surface energy that may be for example, either Griffith- or Barenblatt-like. The implementation of the variational approach to fracture in its original format is a formidable task owing to its nature of free-discontinuity problem and the consequent difficulties emanating from the ambient spaces in which the problem is formulated. Therefore, its numerical implementation¹² has been achieved in *regularized form*, that is, in the form of a damage gradient model for which the damage zone converges to a sharp crack as the length scale parameter tends to zero. In the solid mechanics literature the family of gradient models smoothing the Griffith fracture potential are often referred to as *phase-field models*,^{13,14} and most of them are motivated by the Ambrosio-Tortorelli regularized form¹⁵ of the Mumford-Shah functional used in image segmentation.¹⁶ Common to all these models is the underlying geometrical information consisting in the replacement of the (discrete) fracture surface topology with a fracture surface density function of diffusive type depending on a scalar order parameter, the damage variable, which plays the role of phase field. In the same context, a different point of view is expressed by Freddi and Royer-Carfagni, who present a gradient-regularized damage formulation¹⁷ in the form of an autonomous model amenable to a physical interpretation that goes well beyond a mere mathematical approximation of the parent free-discontinuity problem, the latter being eventually recovered in the limit.

Though from a different perspective, the global energy minimization argument is also exploited by Lorentz,¹⁸ that builds up on previous contributions^{19,20} where the framework of generalized standard materials²¹ has been suitably extended to incorporate models with gradients of internal variables. It bears emphasis that the mentioned extension comes at the expenses of the local normality rule, that is abandoned for gradient-dependent models since it is *overconstraining* on account of the adopted form of the free energy and dissipation functionals. In this respect it is worth recalling that the (usual) normality rule is only sufficient to ensure the satisfaction of the dissipation inequality but it is not a necessary condition. Actually, in the language of Ponter et al.²² it is referred to as *essentially a nonthermodynamic property*. Another variant of the gradient enhancement has been first exploited by Comi²³ via the introduction of spatial derivatives directly in the damage loading function, which acquires then a nonlocal character since it depends on damage and the Laplacian of damage. This interpretation also applies to the gradient model of Lorentz et al.,^{18,24} which appears to be equivalent to a model in which the yield function includes the Laplacian of damage via a non-negative diffusion coefficient with the physical dimensions of a force.

Common to all the aforementioned approach is the fact that, once spatial gradients and/or a length scale are introduced in the constitutive equations, the latter are no longer defined at the local (quadrature point) level but they are established at a larger scale, that is, the scale of the structural model. Basically, for usual local models stresses, strains and internal variables are all defined in a point-wise fashion whereby, their values can be regarded as the parameters of a piece-wise constant interpolation.²⁵ Hence, variables computed at the Gauss point level in classical displacement-based finite element methods are all understood as fields that are generally discontinuous across elements boundaries and inside elements as well. This discontinuous character is indeed one of the most striking consequences of the strictly local character of the constitutive law. Contrariwise, for nonlocal and gradient-enhanced models the presence of gradient or averaging operators in the constitutive equations enforces a greater regularity of strains, stresses and internal variables and the resulting solution will be globally smoothed through elements. Moreover, increased regularity generally characterizes the entire solution and is not limited to the gradient-enhanced variables.

For gradient-enhanced damage models, an important distinction can be made with reference to the form of the enhancement and its relationship with integral nonlocal formulations. In particular, the intrinsically different properties of *explicit* and *implicit* gradient enhancements can be summarized as follows.¹⁰ In explicit gradient models is defined an averaged quantity $\bar{y}(x)$, x being the spatial variable, that may well be a strain-like variable or a measure of elastic energy. This averaged variable is used in the damage constitutive equation to introduce a regularizing effect that avoids ill-posedness of the problem due to strain localization. In the explicit gradient-enhancement the spatially averaged variable is defined as:

$$\bar{y}(x) = y(x) + c\nabla^2 y(x), \quad (1)$$

∇^2 being the Laplace operator.

Since $\bar{y}(x)$ depends on the value and on the derivatives of the function y at point x , this formulation is mathematically local and can be regarded as a higher-order representation of the variable $y(x)$ that is used to describe damage evolution. One major drawback of the representation (1) is that it may require use of $C^{(1)}$ -continuous interpolations, which a priori is not desirable. On the opposite side, implicit gradient models rely upon an equation that looks very similar to (1):

$$\bar{y}(x) - c\nabla^2\bar{y}(x) = y(x) \quad (2)$$

but has quite different properties. In particular, worth mentioning are the reduced interpolation requirement and the fact that higher-order derivatives of $y(x)$ are implicitly still present in the representation of $\bar{y}(x)$, which renders Equation (2) richer in information content compared to (1).

Geers et al.²⁶ have first put forward that the implicit gradient formulation is sometimes deficient in that excessive damage spread may take place in the direction orthogonal to that of a propagating crack as a consequence of the diffusive character of Equation (2). The same conclusion is arrived at in the article by De Borst and Verhoosel,²⁷ where it is explicitly stated that standard gradient damage formulations are not suitable to represent sharp cracks, which in a sense constitutes a clear-cut limitation. A possible remedy to this undesirable feature is to replace in (2) the constant diffusion coefficient c by a strain-dependent activity parameter.²⁶ This results in a more involved procedure to solve the problem equations unless the diffusion equation is reformulated as suggested by Saroukhani et al.,²⁸ whereby the gradient of the strain activity parameter is ruled out from the relevant weak form. Worth mentioning is also the localizing gradient approach of Poh and Sun²⁹ that starts from a different perspective but also ends up with a field equation where nonlocal interactions decrease with damage. We also remind in passing that, despite the fact that the gradient-enhanced variable can be an equivalent strain, when using the implicit gradient model one arrives at a coupled problem for which the inf-sup condition of mixed finite element methods does not apply.³⁰

Restricting attention to phase-field and implicit-type gradient models, in order to solve the problem one has to provide suitable boundary conditions for the gradient-enhanced variable, say κ . Obviously, such boundary conditions have a direct impact on the solution of the problem. A homogeneous Neumann-type boundary condition given as:

$$\frac{\partial \kappa}{\partial \mathbf{n}} = 0 \quad (3)$$

is the almost universally adopted choice, though the question about the physical motivation for it is in most cases left unanswered. Equation (3) can however be recovered as a mere mathematical condition.³¹ In this case a model incorporating the gradient of damage enhancement follows in a natural way from the very definition of mechanical dissipation that, for the class of extended generalized standard materials, is understood as a convex functional of the time rate of the damage field. The above argument supersedes the formulation presented by Frémond and Nedjar⁵ in that it bypasses the completely artificial modification of the principle of virtual power proposed therein, which appears to have been introduced only as a mean to fix the model equations.

In this article we present a gradient-based damage formulation relying upon a local damage description, obeying a normality rule and subject to convex constraints. The model is called *graded damage* to remind the fact that here we do not only penalize the gradient of damage as in phase-field models, but rather we control the magnitude of the gradient of damage by prescribing a suitable bounding function for it. This results in a model that is shown to share many features with the *thick level set* (TLS) approach initially proposed by Moës et al.³² to model the continuous transition between damage and fracture.

In the original TLS formulation the damage state is expressed in an explicit, geometrical fashion as a function of a surrogate variable ϕ , that is, the level set; in particular, level sets allow to track the moving layers of finite thickness l evolving from 0 to l_c where the transition between the sound material and the completely damaged one occurs. Contrariwise, the model presented in this article abandons the level set-based representation in favor of an implicit description of damaged regions, whereby one arrives at a Generalized Standard Model supplemented by two convex constraints. The first one is of local type and expresses the usual $[0,1]$ bounds on the damage variable while the second one is responsible of nonlocality and acts on the gradient of damage by prescribing the shape of damage distribution within the transition layer and the length scale l_c as well.

The structural problem of the elastic-graded damageable body is governed by a three-field functional; this is in turn obtained by introducing a potential of the constraints that allows to define a total potential energy to render stationary with respect to the arguments. The incremental solution of the problem of the elastic-damageable body is therefore characterized as the saddle-point of the potential energy, which is separately convex with respect to displacement and damage

fields. Moreover, the functions governing the degradation of elastic stiffness and the softening part of the constitutive law can be designed to deal with a variety of behaviors using material parameters of clear physical meaning.

The outline of the article is as follows. In Section 2 we introduce the constitutive model and the relevant constraint equations; the graded damage model and its relationship with the TLS approach are developed in Section 3. The structural model and the variational structure of the coupled three-field problem are presented in Section 4, where the distinctive features of the proposed model compared to the TLS formulation are also enlightened. In Section 5 the problem of the one-dimensional rod under tensile load is discussed and the choice of the constitutive functions for the continuum damage formulation is made, motivated by the equivalence with the softening law of a given cohesive relationship. The Finite Element implementation is then outlined in Section 6 while representative numerical examples are documented in Section 7 that demonstrate the capabilities of the proposed approach.

2 | CONSTITUTIVE MODEL

Let us consider an elasto-damaging structural model undergoing a quasi-static loading process whose events are ordered by a pseudo-time scalar parameter t that will be referred to in the remainder as *time*. At each instant $t \in [0, T]$ the current configuration of the body is defined by a simply connected open set $\Omega(t) \subseteq \mathfrak{R}^3$ described by the linear space of its displacements \mathbf{u} from a reference configuration $\Omega(0)$:

$$\mathbf{u}(\mathbf{X}, t) = \chi(\mathbf{X}, t) - \mathbf{X}, \quad (4)$$

which relates the placements \mathbf{X} of the material particles in the reference configuration to the corresponding (deformed) ones $\mathbf{x} = \chi(\mathbf{X}, t)$ occupied at time t in the current configuration through the deformation map χ .

Under the assumption of small transformations the kinematics of deformation is characterized by the infinitesimal strain measure:

$$\boldsymbol{\varepsilon} = \frac{1}{2} (\nabla \mathbf{u} + \nabla \mathbf{u}^T). \quad (5)$$

Addressing the linear isotropic case, the energy density function for the undamaged solid reads:

$$\psi^0(\boldsymbol{\varepsilon}) = \frac{1}{2} [2\mu \boldsymbol{\varepsilon} : \boldsymbol{\varepsilon} + \lambda \text{tr}^2(\boldsymbol{\varepsilon})], \quad (6)$$

μ and λ being the Lamé elastic moduli. Degradation of the stored energy can be introduced in multiplicative form via a monotonically decreasing scalar function $\omega(d)$ of the damage field d that transforms the sound material ($d = 0$) into a fully damaged one ($d = 1$) according to:

$$\omega(0) = 1; \quad \omega(1) = 0. \quad (7)$$

The simplest case consists in assuming a fully symmetric behavior, that is,

$$\psi(\boldsymbol{\varepsilon}, d) = \omega(d) \psi^0(\boldsymbol{\varepsilon}), \quad (8)$$

whereby stiffness and stress degradation occur with no distinction in tension and compression. Obviously, this form of the stored energy neglects crack closure effects and allows to effectively model only cases that are tension-dominated. A nonsymmetric tension-compression behavior can be obtained by splitting the stored energy function as in Miehe et al.:¹³

$$\psi(\boldsymbol{\varepsilon}, d) = \omega(d) \psi_+^0(\boldsymbol{\varepsilon}) + \psi_-^0(\boldsymbol{\varepsilon}), \quad (9)$$

where ψ_\pm^0 are the positive (negative) undamaged shares:

$$\psi_\pm^0(\boldsymbol{\varepsilon}) = \frac{1}{2} [2\mu \boldsymbol{\varepsilon}_\pm : \boldsymbol{\varepsilon}_\pm + \lambda \langle \text{tr}(\boldsymbol{\varepsilon}) \rangle_\pm^2]. \quad (10)$$

In the above equation symbol $\boldsymbol{\varepsilon}_\pm$ denotes the positive (negative) strain tensor that is computed based on the spectral decomposition

$$\boldsymbol{\varepsilon}_{\pm} = \sum_{i=1}^3 \langle \varepsilon_i \rangle_{\pm} \mathbf{n}_i \otimes \mathbf{n}_i, \quad (11)$$

where ε_i and \mathbf{n}_i are eigenvalues and eigenvectors, respectively, and $\langle x \rangle_{\pm}$ stands for the positive (negative) part of the scalar argument x .

An immediate generalization of the stored energy (9) that is also considered by Moës et al.³² can be expressed in the form:

$$\psi(\boldsymbol{\varepsilon}, d) = \omega(d) \left[\psi_+^0(\boldsymbol{\varepsilon}) + h \psi_-^0(\boldsymbol{\varepsilon}) \right], \quad (12)$$

where the scalar parameter $h \in [0, 1[$ is used to manage compressive damage, which is less harmful than tensile damage owing to crack closure. Alternative forms of energy degradation are however possible in which isotropy is preserved and/or the part of strain energy that is affected by damage is associated to expansion and/or shear using different strain splitting schemes.³³

For a local model the forces work-conjugate to the state variables $\boldsymbol{\varepsilon}, d$ follow from the standard thermodynamic argument;³⁴ this provides the Cauchy stress tensor $\boldsymbol{\sigma}$ and the damage energy release rate Y as:

$$\boldsymbol{\sigma} = \frac{\partial \psi(\boldsymbol{\varepsilon}, d)}{\partial \boldsymbol{\varepsilon}} \quad (13)$$

$$Y = - \frac{\partial \psi(\boldsymbol{\varepsilon}, d)}{\partial d}. \quad (14)$$

It is worth emphasizing the physical meaning of the damage energy release rate Y , which represents the elastic energy released per unit volume of damaging material; this is different compared to the usual energy release rate of fracture mechanics that is a surface energy, that is, an energy per unit area of surface cracks. The existing link between the two, that allows to find a scaling relationship between the relevant critical values, depends on the material length scale that characterizes the size of the process-zone bands where damage develops. This aspect is discussed in Section 5 where the constitutive functions of the model are determined in a way to be consistent with a given cohesive law.

2.1 | Introducing constraints

In the present model the damage variable d has to comply with two internal constraints described via convex functions.

The first one is a two-sided constraint of local type and provides the usual bounds for the order parameter describing the state of the material:

$$0 \leq d \leq 1. \quad (15)$$

The above condition can be expressed either using the convex indicator function of the interval $[0,1]$:

$$\mathbb{I}_{[0,1]}(d) = \begin{cases} 0 & \text{if } d \in [0, 1] \\ +\infty & \text{otherwise} \end{cases}, \quad (16)$$

or via a suitably regularized version of it in the form

$$g_1(d) \leq 0, \quad (17)$$

that will be defined later on. The second constraint is one-sided and nonlocal and expresses a bound for the norm of the gradient of damage as:

$$g_2(d) = \|\nabla d\| - f(d) \leq 0. \quad (18)$$

The inequality (18) does strongly characterize the present model that is termed *graded damage* to emphasize the fact that the magnitude of the gradient of damage is explicitly bounded by a positive function, here given as $f(d)$. The spatial gradient term in (18) introduces nonlocality in the formulation whereas information about the length scale and the shape of the damage distribution within the transition zone is contained in the characteristic function $f(d)$. It can be easily shown³⁵ that (18) defines a convex set provided that the function g_2 is convex, that is, if the characteristic function $f(d)$ is concave, which is equivalent to $-f(d)$ convex. The proof is sketched hereafter; to this purpose it assumed that $f(0) > 0$.

Proposition 1. *For any concave function f , if there exists a point d_o such that $f(d_o) > 0$, the set*

$$C = \{(d, \nabla d) \in S / g_2(d) \leq 0\} \quad (19)$$

is a nonempty and convex set in S .

Proof. The set C is nonempty by hypothesis since $(d_o, 0) \in C$. Given a pair of elements of C , that is, $(d, \nabla d)$ and $(d^*, \nabla d^*)$, by definition their convex combination fulfills the condition:

$$\theta \|\nabla d\| + (1 - \theta) \|\nabla d^*\| \leq \theta f(d) + (1 - \theta) f(d^*) \quad (20)$$

for $\theta \in [0, 1]$. On the one hand, for a concave function f one has:

$$\theta f(d) + (1 - \theta) f(d^*) \leq f(\theta d + (1 - \theta) d^*), \quad (21)$$

while, on the other side, it turns out to be

$$\|\theta \nabla d + (1 - \theta) \nabla d^*\| \leq \theta \|\nabla d\| + (1 - \theta) \|\nabla d^*\| \quad (22)$$

by virtue of the triangular inequality.

The previous three relationships provide the condition:

$$\|\theta \nabla d + (1 - \theta) \nabla d^*\| \leq f(\theta d + (1 - \theta) d^*), \quad (23)$$

whereby the convex combination of $(d, \nabla d)$ and $(d^*, \nabla d^*)$ belongs to C , which proves the proposition. ■

The constraints (17) and (18) are introduced in the formulation via two fields of Lagrange multipliers γ_1, γ_2 and the relevant Karush–Kuhn–Tucker (KKT) conditions, that is:

$$\gamma_i \geq 0; \quad g_i(d) \leq 0; \quad \gamma_i g_i(d) = 0. \quad (24)$$

The previous relationships characterize these constraints as nondissipative, whence a potential of (17) and (18) can be formally defined as:

$$\psi_\gamma(d, \gamma_i) = \gamma_1 g_1(d) + \gamma_2 g_2(d), \quad (25)$$

which is convex since it is the linear combination of two convex functions.

3 | THICK LEVEL SETS VERSUS GRADED DAMAGE

The thick level set (TLS) model originally contributed by Moës et al.³² is a nonlocal damage formulation in which the damage variable d is not directly related to the strain or strain energy but is expressed in geometrical terms, that is, as an explicit function of the distance to a moving interface Γ_o representing the damage front, that is the surface separating the damaged and undamaged portions of the domain under consideration. Transition between the sound material and the completely damaged one occurs within layers of finite thickness l_c , which plays the role of a physical length scale that regularizes the damage model by preventing pathological mesh-dependence effects subsequent to strain localization.

In summary, the domain of the damaging body can be partitioned into three distinct regions: the undamaged portion Ω_0 , the interphase or transition layer Ω_c , where the damage variable ranges between 0 and 1, and the completely damaged region Ω_1 , see for example, Figure 1.

In order to continuously track the position of the damage front, that is, the iso-zero damage surface, in the TLS approach use is made of the signed distance function $\phi(\mathbf{X})$ as a surrogate variable. The function $\phi(\mathbf{X})$ is the level set and is computed based on equation

$$\|\nabla\phi(\mathbf{X})\| = 1, \quad \mathbf{X} \in \Omega \quad (26)$$

to which the following boundary condition applies:

$$\phi(\mathbf{X}) = 0, \quad \forall \mathbf{X} \in \Gamma_o. \quad (27)$$

Relationship (26) is an *Eikonal equation*, that is a nonlinear, first-order partial differential equation of Hamilton–Jacobi type. The solution of the Eikonal provides the distance function $\phi(\mathbf{X})$, that is, the length of the shortest path within Ω between points \mathbf{X} and the iso-zero curve Γ_o .

In order to obtain the damage distribution over the domain, a shape function $d(\phi)$ of the distance $\phi(\mathbf{X})$ is designed. This is a peculiar feature of the TLS model that considers the damage shape function as a material property. In particular, points with negative distance from Γ_o are undamaged ($d(\phi) = 0$) whereas points located at a distance greater than l_c are fully damaged ($d(\phi) = 1$). In the transition zone the prescribed damage function $d(\phi)$ is continuously increasing with distance ϕ from the sound material and its derivative along ϕ is strictly positive and bounded by a positive function $f(d)$. These properties are summarized below:

$$\begin{aligned} \mathbf{X} \in \Omega_o, \quad \phi(\mathbf{X}, t) \leq 0, \quad d(\mathbf{X}) = 0 \\ \mathbf{X} \in \Omega_c, \quad 0 \leq \phi(\mathbf{X}, t) \leq l_c, \quad 0 < d'(\phi) < f(d) \\ \mathbf{X} \in \Omega_1, \quad \phi(\mathbf{X}, t) \geq l_c, \quad d(\mathbf{X}) = 1, \end{aligned} \quad (28)$$

having denoted by $d'(\phi)$ the damage derivative along the level set ϕ .

The boundary of the transition zone is $\partial\Omega_c = \Gamma_o \cup \Gamma_1$ and points $\mathbf{X} \in \partial\Omega_c$ fulfill the following:

$$\mathbf{X} \in \Gamma_o, \quad \phi(\mathbf{X}, t) = 0, \quad d(\mathbf{X}) = 0; \quad (29)$$

$$\mathbf{X} \in \Gamma_1, \quad \phi(\mathbf{X}, t) = l_c, \quad d(\mathbf{X}) = 1. \quad (30)$$

Damage evolution is associated to the motion $\dot{\phi}$ of the interface Γ_o and the damage time rate reads:

$$\dot{d} = d'(\phi) \dot{\phi}. \quad (31)$$

The damage time rate is positive owing to irreversibility of damage and is also bounded because such is $d'(\phi)$. The spatial gradient of damage is bounded as well; actually, use of the chain rule yields:

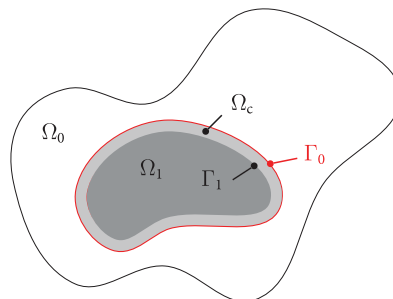


FIGURE 1 Domain partition in the TLS approach

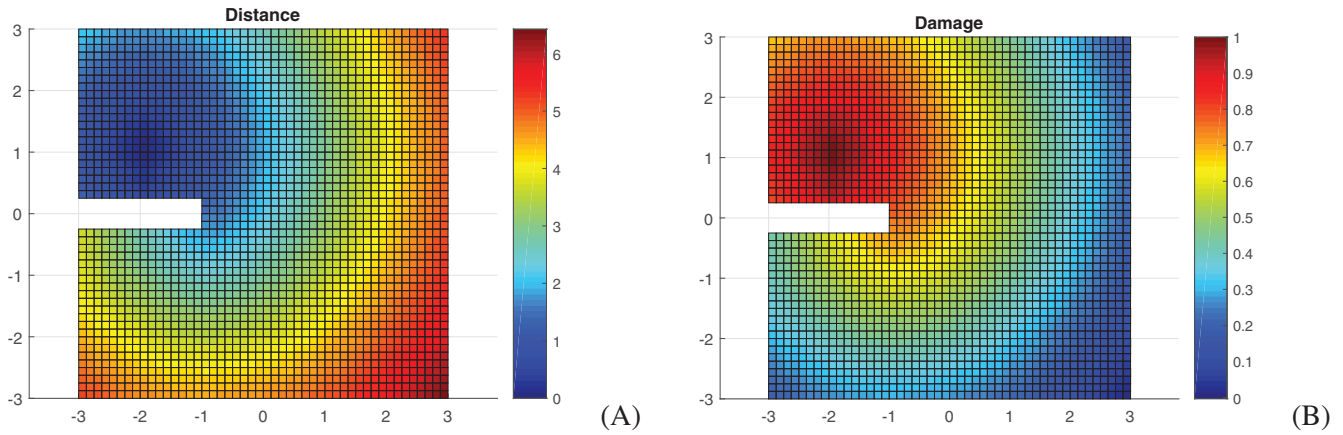


FIGURE 2 Level set (A) and damage field (B) on a notched plate

$$\|\nabla d(\phi(\mathbf{X}))\| = d'(\phi)\|\nabla\phi(\mathbf{X})\|. \quad (32)$$

Within the localization band Ω_c one has therefore:

$$\|\nabla d(\mathbf{X})\| \leq f(d), \quad (33)$$

since ϕ is a distance function and, as such, has unit spatial gradient.

In summary, in terms of the level set $\phi(\mathbf{X})$ the explicit model equations in Ω_c read:

$$d = d(\phi); \quad \|\nabla\phi\| = 1; \quad d'(\phi) \leq f(d). \quad (34)$$

Equation (34) express the original, *geometrical point of view* of the TLS approach. They can be condensed into a single relationship to get the condition (33), which provides the *continuum mechanics point of view* of the graded damage model.

Though apparently very different, the two interpretations have much in common. To show the similarities between them we consider in Figure 2 a variant of the notched plate example.³⁶ In particular, Figure 2A depicts the geodesic distances ϕ on the notched plate computed from point \mathbf{X}_0 of Cartesian coordinates $(-2, 1)$ and obtained from the solution of the Eikonal Equation (26) with boundary condition $\phi(\mathbf{X}_0) = 0$. On Figure 2B is shown the damage distribution on the same domain obtained from the damage equations detailed in next section with $f(d) = 1/l_c$ and $d(\mathbf{X}_0) = 1$ as a Dirichlet boundary condition.

The two pictures do perfectly compare each other in the sense that, except from a scale change, they show the same solution. This originates from the fact that, owing to its properties, the damage shape function $d(\phi)$ admits the inverse $\phi(d)$, whereby in this case the function $f(d)$ in Ω_c can be obtained from $d(\phi)$ as:

$$f(d) = d'(\phi(d)). \quad (35)$$

Therefore, though implicitly, the nonlocal constraint (33) still contains information on the level sets via the spatial gradient of damage and the characteristic function $f(d)$.

4 | THE STRUCTURAL PROBLEM

Based on the previous considerations the reversible behavior of the elasto-damaging body Ω is governed by a global potential energy of the field variables that takes the form of a three-field functional:

$$\mathcal{E}(\mathbf{u}, d, \gamma_i) = \int_{\Omega} \psi(\boldsymbol{\varepsilon}(\mathbf{u}), d) \, d\Omega - \int_{\partial\Omega_t} \mathbf{t} \cdot \mathbf{u} \, dS + \int_{\Omega} \psi_{\gamma}(d, \gamma_i) \, d\Omega, \quad (36)$$

where ψ is the stored energy function and ψ_{γ} the constraint potential (25).

On the other hand, for a Generalized Standard model damage evolution emanates from a global pseudo-potential of dissipation; this is in turn a non-negative closed convex functional that is obtained by integrating a local dissipation function φ over the domain Ω :

$$\mathcal{D}(d^*) = \int_{\Omega} \varphi(d^*) \, d\Omega. \quad (37)$$

Rate-independent behavior requires the dissipation function φ be positively homogeneous of degree one with respect to the damage time rate d^* . A possible expression for φ is:

$$\varphi(d^*) = Y_c(d) d^* + \mathbb{I}_{\mathbb{R}^+}(d^*), \quad (38)$$

where $Y_c(d)$ is a positive convex function of the current damage state d , here considered as a parameter, that provides the instantaneous elastic limit; $\mathbb{I}_{\mathbb{R}^+}$ is the convex indicator function of non-negative reals:

$$\mathbb{I}_{\mathbb{R}^+}(d^*) = \begin{cases} 0 & \text{if } d^* \geq 0 \\ +\infty & \text{otherwise} \end{cases} \quad (39)$$

that enforces damage irreversibility.

4.1 | Equilibrium

For given damage state d and Lagrange multipliers γ_i , the displacement field at solution is a minimizer for the potential energy over the set of kinematically admissible displacements \mathcal{U} defined as:

$$\mathcal{U} = \{ \mathbf{u}^* \mid \mathbf{u}^*(\mathbf{X}) = \mathbf{u}^d(\mathbf{X}), \mathbf{X} \in \partial\Omega_u \}, \quad (40)$$

where $\partial\Omega_u$ denotes the Dirichlet boundary; the complementary part $\partial\Omega_t$ of $\partial\Omega$ is the Neumann boundary, where surface tractions \mathbf{t} are prescribed.

In particular, the equilibrium equations are obtained by zeroing the first variation of the potential (36) with respect to \mathbf{u} as:

$$\frac{\partial \mathcal{E}}{\partial \mathbf{u}} \cdot \delta \mathbf{u} = 0, \quad \forall \delta \mathbf{u} \in \{ \mathbf{v} \mid \mathbf{v}(\mathbf{X}) = 0, \mathbf{X} \in \partial\Omega_u \}. \quad (41)$$

The above equation embodies the definition (13) of the Cauchy stress and the differential equilibrium equation along with the relevant static boundary condition:

$$\operatorname{div} \boldsymbol{\sigma} = 0, \quad \text{in } \Omega; \quad \boldsymbol{\sigma} \mathbf{n} = \mathbf{t}, \quad \text{on } \partial\Omega_t. \quad (42)$$

4.2 | Domain partition

Variations of the potential energy with respect to the Lagrange multipliers read:

$$\begin{aligned} \frac{\partial \mathcal{E}}{\partial \gamma_1} \delta \gamma_1 &= \int_{\Omega} g_1(d) \delta \gamma_1 \, d\Omega, \\ \frac{\partial \mathcal{E}}{\partial \gamma_2} \delta \gamma_2 &= \int_{\Omega} g_2(d) \delta \gamma_2 \, d\Omega. \end{aligned} \quad (43)$$

The above relationships allow to identify a decomposition of the domain Ω according to the state of internal constraints, that is, the sign of the constraint functions g_1 and g_2 .

In particular, for a *compatible damage state* d the variations (43) are both nihil and the domain Ω can be partitioned as follows (see also Figure 1):

$$\Omega = \Omega_o \cup \Omega_c \cup \Omega_1 \quad (44)$$

with the properties:

- i) on Ω_o and Ω_1 the damage field exactly meets the lower and upper bounds, respectively, whereby $g_1 = 0$ and, consequently, γ_1 can take any value;
- ii) on Ω_c damage is strictly comprised within bounds ($g_1 < 0$), whence $\gamma_1 = 0$;
- iii) on Ω_o and Ω_1 there is no damage activity since the gradient of damage has zero magnitude; therefore $g_2 = -f(d) \leq 0$ and $\gamma_2 = 0$.

The domain Ω_c where progressive damage develops can in turn be partitioned into two subdomains:

- iv) Ω_c^- where the norm of the damage gradient is strictly lower than $f(d)$, whereby $g_2 < 0$ and $\gamma_2 = 0$;
- v) Ω_c^o where the gradient of damage exactly meets the condition $g_2 = 0$ and γ_2 can take any value.

For an *arbitrary damage distribution* that is not a converged state of the system constraints (17) and (18) are generally not fulfilled everywhere in Ω and regions where the integrals (43) are positive may exist. These incompatible regions do represent the active constraint set where the Lagrange multipliers have to be adjusted during the solution process in order to restore compatibility.

4.3 | Damage-driving forces

The thermodynamic forces responsible of damage evolution are obtained by computing the first variation of the potential (36) with respect to d :

$$\delta \mathcal{E} = \int_{\Omega} \left[\frac{\partial \psi}{\partial d} \delta d + \gamma_1 g'_1(d) \delta d + \gamma_2 \left(\frac{\nabla d}{\|\nabla d\|} \cdot \nabla \delta d - f'(d) \delta d \right) \right] d\Omega, \quad (45)$$

where the scalar functions $g_1(d)$ and $f(d)$ have been left unspecified at this stage since they are of local type and their particular form does not affect the nature of the problem at hand.

The gradient-dependent term in Equation (45) can be transformed using the divergence theorem to obtain:

$$\frac{\partial \mathcal{E}}{\partial d} \delta d = - \int_{\Omega} G \delta d \, d\Omega + \int_S \left[\gamma_2 \frac{\nabla d}{\|\nabla d\|} \right]_S \cdot \mathbf{n} \delta d \, dS + \int_{\partial\Omega} \gamma_2 \frac{\nabla d}{\|\nabla d\|} \cdot \mathbf{n} \delta d \, dS. \quad (46)$$

The three terms put forward in the previous relationship are as follows. The volume integral defines the damage energy release rate G as:

$$G = Y - \gamma_1 g'_1(d) + \gamma_2 f'(d) + \operatorname{div} \left(\gamma_2 \frac{\nabla d}{\|\nabla d\|} \right). \quad (47)$$

The thermodynamic force G is of nonlocal type whenever $\gamma_2 \neq 0$ because of the divergence term originating from the constraint Equation (18); as shown in Section 4.2 this can occur only in region Ω_c^o where $g_2(d) = 0$. On the contrary, in the other regions one has $\gamma_2 = 0$ and the gradient-dependence is dropped out, whereby G is a local quantity.

The integral over internal, possible discontinuity surfaces S is assumed to be nihil, that corresponds to the nondissipative case:

$$\left[\gamma_2 \frac{\nabla d}{\|\nabla d\|} \right]_S \cdot \mathbf{n} = 0. \quad (48)$$

In particular, Equation (48) has to be fulfilled over the surface Γ_o separating Ω_o and Ω_c ; here $d = 0^+$ and $\|\nabla d\| = f(0^+) > 0$, which in turn implies $\gamma_2 = 0$. Along an internal discontinuity surface for the gradient of damage, where d is a continuous function and $g_2 = 0$, that is:

$$\begin{aligned} d^+ &= d^- \\ \|\nabla d^+\| - f(d^+) &= \|\nabla d^-\| - f(d^-) = 0 \end{aligned} \quad (49)$$

one has:

$$\begin{aligned} \mathbf{n} \cdot \nabla d^+ + \mathbf{n} \cdot \nabla d^- &= 0, \\ (\gamma_2^+ \nabla d^+ - \gamma_2^- \nabla d^-) \cdot \mathbf{n} &= 0, \\ \gamma_2^+ &\geq 0; \quad \gamma_2^- \geq 0, \end{aligned} \quad (50)$$

whereby $\gamma_2^+ = \gamma_2^- = 0$. In particular, on the boundary $\partial\Omega_c^- \cap \partial\Omega_c^o$, that is, the surface separating the contiguous regions Ω_c^- and Ω_c^o , the gradient ∇d is discontinuous and therefore $\gamma_2 = 0$.

The surface integral over the external boundary provides the boundary condition for the damage field equation as:

$$\gamma_2 \frac{\nabla d}{\|\nabla d\|} \cdot \mathbf{n} = 0. \quad (51)$$

It is worth emphasizing that the above relationship is more general compared to the usual homogeneous natural boundary condition of phase-field or gradient-enhanced damage models. Actually, the presence of the Lagrange multiplier γ_2 in Equation (51) allows for a nonzero normal derivative of damage on the outer boundary $\partial\Omega$. In particular, on the portion of boundary $\partial\Omega \cap \partial\Omega_c^-$ relationship $g_2 < 0$ holds, which in turn implies $\gamma_2 = 0$.

4.4 | Dissipation and damage evolution

Since the constraints (17) et (18) are nondissipative, the only contribution to the total dissipation of the system originates from the local damage energy release rate Y , that is:

$$-\frac{\partial \mathcal{E}}{\partial d} \dot{d} = \int_{\Omega} G \dot{d} \, d\Omega = \int_{\Omega} Y \dot{d} \, d\Omega \geq 0. \quad (52)$$

Following Germain et al.,³⁷ the irreversible behavior of the structural model is governed by the subdifferential inclusion:

$$-\frac{\partial \mathcal{E}}{\partial d} \in \partial \mathcal{D}(\dot{d}), \quad (53)$$

that generalizes the classical Biot equation to the nonsmooth case. This is indeed the case of the functional \mathcal{D} defined by Equation (37), which is convex but non differentiable due to the presence of the indicator function in (38). The local dissipation function (38) and its subdifferential:

$$\partial \varphi(d^*) = Y_c(d) + \partial \mathbb{1}_{\mathfrak{R}^+}(d^*) \quad (54)$$

are depicted in Figure 3 for a given damage state, that clearly shows their multivalued character.

Relationship (53) embodies the normality rule that governs damage evolution for generalized standard models:

$$G - Y_c(d) \leq 0, \quad \dot{d} \geq 0, \quad (G - Y_c(d)) \dot{d} = 0. \quad (55)$$

On account of the definition of the damage energy release rate G , which may depend upon spatial derivatives of the damage field, the normality law can be characterized as a differential problem. In particular, this occurs in region Ω_c^o where the Lagrange multiplier γ_2 is nonzero and $\|\nabla d\| = f(d)$ since $g_2(d) = 0$. In this case the divergence term of (47)

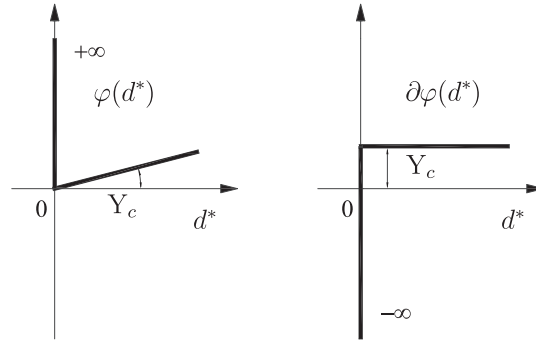


FIGURE 3 Dissipation function and its subdifferential

becomes:

$$\operatorname{div} \left(\gamma_2 \frac{\nabla d}{f(d)} \right) = \frac{1}{f(d)} (\nabla \gamma_2 \cdot \nabla d + \gamma_2 \nabla^2 d) - \gamma_2 f'(d), \quad (56)$$

whereby the normality law (55) can be stated as:

$$\begin{cases} (Y - Y_c(d))f(d) + \operatorname{div}(\gamma_2 \nabla d) \leq 0 \\ \dot{d} \geq 0 \\ [(Y - Y_c(d))f(d) + \operatorname{div}(\gamma_2 \nabla d)] \dot{d} = 0 \end{cases} \quad (57)$$

to which the boundary conditions (48) and (51) apply. It bears emphasis that in relationships (57) there is no dependence on the multiplier γ_1 since the latter is identically zero in Ω_c , and in particular in Ω_c^o . Conversely, in regions Ω_o and Ω_1 the dependence upon γ_2 is dropped out and damage evolution is governed by a purely local law.

It is also interesting to note that the graded damage model is consistent with the case of linear elastic fracture mechanics. To show this it is sufficient to consider the case of a constant Y_c , which allows to define a global functional of dissipated energy:

$$\mathcal{G}(d) = \int_{\Omega} \left(\int_0^d Y_c \, d\alpha \right) \, d\Omega = \int_{\Omega} Y_c d \, d\Omega, \quad (58)$$

whereby the total energy of the system follows as:

$$\mathcal{W}(\mathbf{u}, d, \gamma_i) = \mathcal{E}(\mathbf{u}, d, \gamma_i) + \mathcal{G}(d) \quad (59)$$

and normal damage evolution can be recast in the form of a variational inequality:

$$\dot{d} \geq 0, \quad \frac{\partial \mathcal{W}}{\partial d} (\delta d - \dot{d}) \geq 0, \quad \forall \delta d \geq 0. \quad (60)$$

Equivalence with the TLS model can also be proved. To this end we compute hereafter the integral of the partial differential equation resulting from the normality law (55) that holds in Ω_c^o for $\dot{d} > 0$:

$$(Y - Y_c(d))f(d) + \operatorname{div}(\gamma_2 \nabla d) = 0 \quad (61)$$

to show that one can recover the limit condition of the TLS model that is expressed in terms of the energy release rate associated to the motion of a layer of thickness l :³⁸

$$\hat{G} = \int_0^l Y d'(\phi) j(\phi) \, d\phi. \quad (62)$$

In this respect the following considerations are in order. Let $\mathbf{X}_0(a, b)$ be a point belonging to Γ_0 and $\mathbf{X} \in \Omega_c^0$ a point of coordinates (a, b, z) :

$$\mathbf{X}(a, b, z) = \mathbf{X}_0(a, b) + z \nabla \phi, \quad (63)$$

having denoted by z the (positive) coordinate in the direction normal to the iso-damage surface $d = 0^+$ to which \mathbf{X}_0 belongs. In the previous relationship ϕ is the signed distance function from the iso-zero damage surface Γ_0 with unit normal

$$\nabla \phi = \frac{\nabla d}{f(d)}, \quad (64)$$

since, by definition, on Ω_c^0 one has $g_2(d) = 0$ whereby

$$d'(\phi) = f(d). \quad (65)$$

Now consider the truncated cone of axis $\nabla \phi$ depicted in Figure 4 delimited by the area elements $dS(0)$ located at $z = 0$ and $dS(z) = j(z) dS(0)$ located at $z = l$, where the function $j(z)$ accounts for area change due to the local geometric curvature of the surfaces. Integration of the nonlocal term $\text{div}(\gamma_2 \nabla d)$ over the thickness l of the truncated cone Ω_l , which coincides with the thickness of Ω_c^0 , and use of the divergence theorem gives:

$$\int_0^l \text{div}(\gamma_2 \nabla d) j(z) dS dz = [\gamma_2 \nabla d j(z) dS]_{z=0}^{z=l} = 0, \quad (66)$$

since $\gamma_2 = 0$ on the surfaces $dS(z = 0)$ and $dS(z = l)$ because they correspond to the boundary of Ω_c^0 .

With this result in hand, integration of Equation (61) over the truncated cone provides the condition for damage evolution introduced by Moës et al.:³²

$$\hat{G} = \int_0^l Y d'(\phi) j(\phi) d\phi = \int_0^l Y_c(d) d'(\phi) j(\phi) d\phi = \hat{G}_c, \quad (67)$$

where use has been made of (65), the normal coordinate z has been replaced with the level set ϕ (they here coincide) and the area element dS that should multiply all the integrals has been dropped out for notational simplicity.

It is worth emphasizing that, for each point \mathbf{X} , the product $Y d'(\phi)$ appearing in Equation (67) provides the derivative of the stored energy function (9) with respect to the distance ϕ to the damage front Γ_0 ; therefore, the physical meaning of this product is that of local energy release rate corresponding to the motion of the damage front at point \mathbf{X} .

The previous discussion shows that the coupling of a local damage model with the constraint Equation (18) allows one to recover the features of the TLS model in its original, geometrical format. However, the great advantage of the

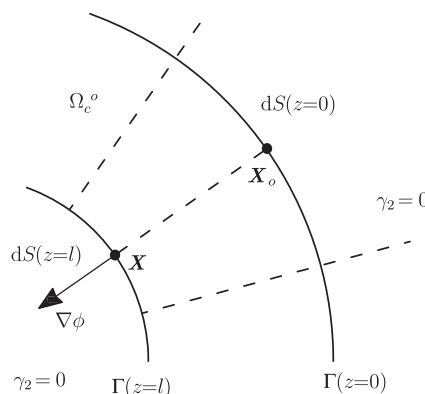


FIGURE 4 Geometry of layers and domain of integration (truncated cone)

graded damage model compared to the TLS formulation is that it can be implemented with no use at all of level sets since Equation (61), which provides the nonlocal damage evolution, is completely independent from the notion of distance function, which has to be understood only as a surrogate variable rather than an essential ingredient of the moving thick layer approach.

5 | A PROBLEM IN ONE DIMENSION: CONSTITUTIVE FUNCTIONS SETUP

This section is devoted to the characterization of the constitutive functions $\omega(d)$ and $Y_c(d)$ that have been left unspecified until now; the goal will be pursued by establishing an equivalence between the present continuum damage formulation and the softening law of a cohesive zone model in the wake of similar analyses conducted in the literature.^{18,39,40}

To this end we shall refer to the problem of a traction bar in one-dimension, for which a closed-form solution can be readily obtained; this solution may be considered representative of the response of a two- or three-dimensional structure across a localization band. The domain occupied by the rod is the interval $[-L, L]$, body forces are neglected and loading is performed by prescribing the axial displacement u at the two ends of the bar as:

$$u(-L) = -u^*, \quad u(L) = u^*; \quad u^* > 0. \quad (68)$$

The stress is uniform along the bar by equilibrium:

$$\sigma = \omega(d) E \frac{du}{dx}, \quad (69)$$

E being the elastic modulus; the free energy and the dissipation function are taken by analogy with their three-dimensional counterparts (12) and (38), whereby one has a normality rule in the form (55). The nonlocal constraint function is taken as:

$$g_2(d) = \left| \frac{dd}{dx} \right| - \frac{1}{l_c} \quad (70)$$

to which the following KKT conditions apply:

$$g_2(d) \leq 0; \quad \gamma \geq 0; \quad \gamma g_2(d) = 0, \quad (71)$$

whence results a piece-wise linear distribution of damage along the rod.

During the loading phase, when the displacement u^* initially grows from 0 to the elastic limit, the unique possible response is the homogeneous elastic one; afterwards loading is parameterized in terms of the maximum damage level $d_m \leq 1$.

The relationship between the stress and the prescribed displacement reads:

$$2 u^* = \frac{\sigma}{E} \int_{-L}^{+L} \omega^{-1}(d(x)) dx \quad (72)$$

and it can be made explicit once the damage distribution $d(x)$ has been determined.

For the homogeneous inelastic case, damage evolution corresponds to an increase of strain energy everywhere in the bar; this provides a necessary condition for local stability as:

$$Y_c(d) \omega''(d) - Y_c'(d) \omega'(d) > 0, \quad (73)$$

where differentiation is made with respect to the damage variable d . The above condition is suggested by Lorentz¹⁸ along with the one emanating from strain softening, according to which the complementary elastic energy should decrease with damage:

$$[Y_c'(d) \omega^2(d) + Y_c(d) 2 \omega(d) \omega'(d)] \omega'(d) - Y_c(d) \omega^2(d) \omega''(d) \geq 0. \quad (74)$$

Without loss of generality, for the case of nonhomogeneous damage we assume that one single defect initiates at point $x = 0$ right after the initial elastic limit, so that the analysis can be restricted to half of the bar. Owing to (71), the Lagrange multiplier γ can be nonzero only on the active constraint set Ω_c^0 , that is, where $g_2(d) = 0$; in this case the damage function reads:

$$d(x) = d(0) \left(1 - \frac{x}{l_m} \right) = d_m - \frac{x}{l_c}, \quad (75)$$

$l_m = d_m l_c$ being the half-width of the localization band. For damage evolution one has then the first-order ordinary differential equation:

$$\frac{-\omega'(d)}{\omega^2(d)} \frac{\sigma^2}{2E} + \frac{1}{l_c} \gamma'(d) = Y_c(d) \quad (76)$$

to which two boundary conditions apply, one for the stress and another for the differential equation itself. Integration of (76) between 0 and d_m provides:

$$\sigma^2(d_m) = \frac{2E}{\omega^{-1}(d_m) - 1} \int_0^{d_m} Y_c(\alpha) d\alpha, \quad (77)$$

where $Y_c(d)$ is the softening function to be determined. To this end re-write Equation (72) for the half bar and split the integral into two parts, respectively accounting for damage behavior and a purely elastic response:

$$u^* = \frac{\sigma}{E} \left[\int_0^{l_m} [\omega^{-1}(d(x)) - 1] dx + L \right] = \frac{1}{2} w + \frac{\sigma L}{E}, \quad (78)$$

whereby one can express the apparent opening displacement w across the localization band in terms of the chosen parameterization as:

$$w(d_m) = \frac{2\sigma(d_m)}{E} \int_0^{l_m} [\omega^{-1}(d(x)) - 1] dx = \frac{2\sigma(d_m)}{E} l_c F(d_m). \quad (79)$$

Relationships (77) and (79) are used to determine the function $Y_c(d)$ by requiring that the response of the damageable rod be equivalent to that of an elastic bar endowed with a cohesive interface. For example, consider the linear softening relationship:

$$f(w) = \sigma_f - \frac{\sigma_f^2}{2G_f} w, \quad (80)$$

where σ_f and G_f respectively denote the peak stress and the surface fracture energy. Substituting (79) into (80) and solving for σ provides the stress as:

$$\sigma(d_m) = \frac{\sigma_f}{1 + \lambda F(d_m)}, \quad (81)$$

where λ is a nondimensional parameter expressing the ratio between the characteristic length l_c of the graded damage model and the length scale of the cohesive zone:

$$\lambda = \frac{l_c \sigma_f^2}{E G_f}. \quad (82)$$

For a given d_m , substitution of (81) into (77) yields:

$$\int_0^{d_m} Y_c(d) dd = \frac{\omega^{-1}(d_m) - 1}{2E} \left(\frac{\sigma_f}{1 + \lambda F(d_m)} \right)^2. \quad (83)$$

The above equation clearly shows that the constitutive function $Y_c(d)$ depends both on the given cohesive softening law (80) and on the stiffness degradation function $\omega(d)$.

At least in principle, any monotonically decreasing function that continuously maps the scalar damage variable d onto the interval $[0, 1]$ could be used for $\omega(d)$. Therefore, it is not surprising that no general agreement exist on what the best choice could be. In our view, the form of this function should be either dictated by the mathematics or motivated by the need of ruling out harmful behaviors that can be detected in basic problems such as the tensile rod under consideration.

In the family of phase-field models originated by the Ambrosio–Tortorelli functional, the quadratic degradation function naturally arises from the regularization; these models generally behave in a very smooth manner because high gradients of damage are penalized and the dissipation vanishes for highly damaged regions because so does the source term of the diffusion equation. The quadratic degradation function is also recommended by Miehe et al.^{13,14} in order to comply with the condition

$$\omega'(1) = 0, \quad (84)$$

whereby the damage-driving force converges to a finite value in the fully damaged state. On the other hand, Lorentz et al.^{18,41} suggest to use a power law with exponent $m \geq 2$ for the degradation function in order to ensure that the average strain across a localization band increases monotonically with damage. On the contrary, the linear degradation function that is classically used in strain-based gradient models seems to be motivated by the suggestive physical picture of damage given by Lemaitre and Chaboche⁴² that translates into the so-called principle of strain equivalence, see for example, the article of Peerlings et al.,³ among others. In this case, the instantaneous dissipation still vanishes at complete damage because for a fully damaged state no further evolution of damage is possible, but the damage-driving force will keep increasing with strain because it is not affected by the degradation function. Therefore, in the model with linear degradation one can more likely obtain damage spread with increasing strain. Moreover, in the model of Peerlings et al.³ the gradient enhancement affects a nonlocal equivalent strain measure and damage is an explicit function of it; use of linear or quadratic degradation would thus make a minor difference.

For the developments that follow and in the subsequent numerical applications we shall use the quadratic function:

$$\omega(d) = (1 - d)^2. \quad (85)$$

This choice is motivated based on stability arguments developed later on in this section. Use of (85) yields:

$$F(d_m) = \frac{d_m^2}{1 - d_m}, \quad (86)$$

whereby one gets the following expressions for the (uniform) stress:

$$\sigma(d_m) = \sigma_f \frac{1 - d_m}{\lambda d_m^2 + 1 - d_m} \quad (87)$$

and for the target constitutive function:

$$Y_c(d) = \frac{\sigma_f^2}{E} \frac{1 + \lambda d^2(d - 3)}{(\lambda d^2 + 1 - d)^3}. \quad (88)$$

Based upon the above results the Lagrange multiplier field γ can be readily obtained by integrating relationship (76). As for the value of λ to be used in computations, it should be taken in a way to comply with conditions (73) and (74); for the case at hand it can be shown that any positive value of λ lower than $1/2$ allows to fulfill both conditions for all $d \in [0, 1]$.

For a given damage distribution the relationship between the stress and the end displacement u^* follows from Equation (72) as:

$$\sigma = \frac{E u^*}{L} \frac{1 - d_m}{(\beta d_m^2 + 1 - d_m)} \quad (89)$$

with

$$\beta = \frac{l_c}{L}. \quad (90)$$

The response of the elasto-damaging rod is clearly dependent from l_c , from the length scale of the cohesive law and from the size of the bar. Actually, comparison of Equation (87) with (89) yields:

$$u^*(d_m) = \frac{\sigma_f L}{E} \frac{\beta d_m^2 + 1 - d_m}{\lambda d_m^2 + 1 - d_m}. \quad (91)$$

The previous relationship allows to obtain the condition under which the response of the rod is stable under displacement control. This occurs if the end displacement u^* is an increasing function of the maximum damage level d_m , which requires in turn:

$$L < \frac{E G_f}{\sigma_f^2}. \quad (92)$$

The above condition strongly depends upon the expressions (85) and (88) assumed for the constitutive functions. For instance, taking for Y_c the constant function, that is, $Y_c(d) = Y_c(0)$, along with the quadratic degradation function (85) one arrives at:

$$\sigma(d_m) = \frac{2 \sigma_f (1 - d_m)}{\sqrt{4 - 2 d_m}} \quad (93)$$

in place of (87) and to

$$u^*(d_m) = \frac{\sigma_f L}{E} \frac{2(\beta d_m^2 + 1 - d_m)}{\sqrt{4 - 2 d_m}} \quad (94)$$

instead of (91). Stability under displacement control now requires:

$$\beta > \frac{3 - d_m}{d_m (8 - 3 d_m)}, \quad (95)$$

whereby one infers that there is always a snap back right after the elastic limit regardless of the size of the rod since the right-hand side of (95) diverges for $d_m \rightarrow 0$. This can slow down convergence in the solution of a finite element problem and should be avoided as much as possible. However, an even more harmful situation is obtained taking the linear degradation function and a constant elastic limit. In this last case stability under displacement control requires:

$$\beta > \frac{1}{\ln(1 - d_m) + 3 d_m} \quad (96)$$

but the right-hand side of the above equation diverges for both $d_m \rightarrow 0$ and for d_m close to 0.94.

6 | FINITE ELEMENT IMPLEMENTATION

The graded damage model presented so far has been numerically implemented using a multifield finite element method. In the adopted computational scheme, which is quite classical for coupled problems, two variational problems are solved via alternate minimization with respect to displacements and damage and maximization with respect to the Lagrange multipliers.

The point of departure is the standard weak form of equilibrium in Galerkin form:

$$-\int_{\Omega} \boldsymbol{\sigma} \cdot \nabla \mathbf{w} \, d\Omega + \int_{\partial\Omega_f} \mathbf{t} \cdot \mathbf{w} \, dS = \mathbf{0} \quad \forall \mathbf{w} \in \mathcal{V}. \quad (97)$$

The set of admissible displacements variations \mathcal{V} is a linear space and no special treatment is needed to solve the above equation for a given damage state. Contrariwise, for given displacements the damage updating step requires the regularization of indicator functions and of internal constraints to render all functions differentiable. To this end use is made of an augmented Lagrangian formulation; this choice has many well-known advantages and leads to a solution scheme that benefits of a considerable robustness.⁴³

Let us first consider the irreversibility condition that has been introduced in (38) via the indicator function (39), which is convex nondifferentiable. The unilateral constraint $\dot{d} > 0$ can be conveniently expressed as:

$$g_3(d) = \xi_d - d \leq 0, \quad (98)$$

supplemented by the KKT conditions

$$\gamma_3 \geq 0; \quad \gamma_3 g_3(d) = 0, \quad (99)$$

where ξ_d is a local history damage field:

$$\xi_d(\mathbf{X}) = \max_{\tau \leq t} d(\mathbf{X}, \tau). \quad (100)$$

Inequality (98) implicitly contains also the constraint $d \geq 0$, that is therefore redundant once (98) has been specified. Therefore, both constraints (17) and (18) become one-sided inequalities specified as:

$$\begin{aligned} g_1(d) &= d - 1 \leq 0 \\ g_2(d) &= \|\nabla d\| - \frac{1}{l_c} \leq 0 \end{aligned} \quad (101)$$

that provide the upper bounds for the damage field and its gradient. The spatial distribution of damage introduced via the nonlocal constraint should be intended as a material property and chosen in accordance with experiments,⁴⁴ whenever available. However, for the problems that are being examined in Section 7 the choice of a constant gradient is motivated by computational convenience only, in that the resulting damage distribution can be exactly represented with bilinear shape functions.

It is also worth emphasizing that the Lagrange multipliers associated to functions g_1 and g_3 cannot be active at the same point \mathbf{X} and at the same time t , whereby a unique multiplier can be used associated to the constraint set

$$\mathcal{K} = \{d \mid 0 \leq d(t_{n-1}) \leq d(t) \leq 1\} \quad (102)$$

whose indicator function can be expressed in regularized form as:

$$A_1(d, \gamma_1) = \frac{1}{2\eta_1} \left[(\gamma_1 + \eta_1 g_1^+(d))^2 + (\gamma_1 + \eta_1 g_3^+(d))^2 - \gamma_1^2 \right], \quad (103)$$

where η_1 is a penalty parameter and g_i^+ are the constraint functions:

$$g_i^+(d) = \max \left\{ g_i(d), -\frac{\gamma_1}{\eta_1} \right\}, \quad (104)$$

that replace the original functions $g_i(d)$ in order to convert into equalities the inequality constraints.⁴⁵ The same regularization is used for the nonlocal constraint expressed via the function g_2 , for which the relevant potential is analogous to (103):

$$A_2(d, \gamma_2) = \frac{1}{2 \eta_2} \left[(\gamma_2 + \eta_2 g_2^+(d))^2 - \gamma_2^2 \right]. \quad (105)$$

Using the above relationships the weak form of the damage evolution equation in regularized form can be expressed as:

$$\int_{\Omega} [c(d) \zeta + \mathbf{C}(d) \cdot \nabla \zeta] \, d\Omega = 0 \quad \forall \zeta \in L^2(\Omega) \quad (106)$$

with:

$$c(d) = -Y(d) + Y_c(d) + [\eta_1 g_1^+(d) + \gamma_1] - [\eta_1 g_3^+(d) + \gamma_1] \quad (107)$$

$$\mathbf{C}(d) = [\eta_2 g_2^+(d) + \gamma_2] \tilde{\mathbf{n}} \quad (108)$$

$$\tilde{\mathbf{n}} = \frac{\nabla d}{\|\nabla d\|}, \quad (109)$$

ζ being the test functions for the damage field.

The displacement field \mathbf{u} and the damage field d are discretized as:

$$\mathbf{u}^h = \sum_{I=1}^{nel} N_I^u \mathbf{a}_I = \mathbf{N}^u \mathbf{a}; \quad d^h = \sum_{I=1}^{nel} N_I^d \mathbf{m}_I = \mathbf{N}^d \mathbf{m} \quad (110)$$

using standard $C^{(0)}$ interpolations since strains and damage gradients are allowed to be discontinuous. In the present implementation the same interpolations are used for the trial functions \mathbf{w} and ζ whereas Lagrange multipliers are evaluated at quadrature points of the elements, thus implicitly assuming a piece-wise constant interpolation within the elements themselves. In this way the number of global dofs of the problem is not directly affected by the multipliers, that are updated using the classical Hestenes–Powell first-order formula:⁴⁶

$$\gamma_i^{(k+1)} = \gamma_i^{(k)} + \eta_i g_i^+(d), \quad (111)$$

which follows from definitions (103) and (105) of the regularized constraint potentials by zeroing the first variation with respect to the multipliers. Substitution of the interpolations (110) into (97) and (106) results into two coupled residual equations:

$$\begin{aligned} - \int_{\Omega} \mathbf{B}^{u,T} \boldsymbol{\sigma} \, d\Omega + \int_{\partial\Omega} \mathbf{N}^{u,T} \mathbf{t} \, dS &= \mathbf{0}, \\ \int_{\Omega} [\mathbf{B}^{d,T} \mathbf{C}(d) + \mathbf{N}^{d,T} c(d)] \, d\Omega &= \mathbf{0}, \end{aligned} \quad (112)$$

where \mathbf{B}^u and \mathbf{B}^d denote the standard gradient matrices and the superscript T stands for transpose.

The residuals (112) are both nonlinear owing to the internal constraints and to the adopted form (9) of the local free energy function that accounts for nonsymmetric tensile-compressive behavior. For this reason the Finite Element equations have to be linearized and solved incrementally within the time interval of interest.

The mechanical tangent needed for a full Newton solution reads:

$$\mathbf{K}^u = \int_{\Omega} \mathbf{B}^{u,T} \left(\omega(d) \frac{\partial^2 \psi_+^0}{\partial \boldsymbol{\varepsilon}^2} + \frac{\partial^2 \psi_-^0}{\partial \boldsymbol{\varepsilon}^2} \right) \mathbf{B}^u \, d\Omega, \quad (113)$$

which can be explicitly computed in intrinsic form by differentiating the stress eigenvalues and eigenprojectors.⁴⁷ For the damage problem one has:

$$\mathbf{K}^d = \int_{\Omega} (\mathbf{B}^{d,T} \boldsymbol{\Xi} \mathbf{B}^d + \vartheta \mathbf{N}^{d,T} \mathbf{N}^d) \, d\Omega \quad (114)$$

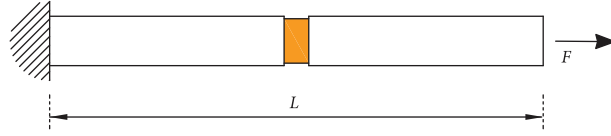


FIGURE 5 Imperfect bar in tension. Model problem

being:

$$\mathbf{\Xi} = \kappa_2 \eta_2 (\tilde{\mathbf{n}} \otimes \tilde{\mathbf{n}}) + \frac{\gamma_2 + \eta_2 g_2(d)}{\|\nabla d\|} (\mathbf{I} - \tilde{\mathbf{n}} \otimes \tilde{\mathbf{n}}) \quad (115)$$

and

$$\vartheta = (\kappa_1 + \kappa_3) \eta_1 - Y'(d) + Y'_c(d) \quad (116)$$

with $\kappa_i = 1$ for $g_i^+(d) > 0$, $i = 1, 3$ and vanishing otherwise.

7 | NUMERICAL EXAMPLES

The numerical simulations documented hereafter refer to the isotropic scalar damage model with nonsymmetric tension-compression behavior described by the free energy (9). Unlike the level set-based approach of Moës et al.,³² in the present implementation we assume the quadratic degradation function (85), that guarantees better stability properties compared to the linear one, see also the discussion in Section 5.

The characteristic function that is used to bound the norm of the gradient of damage is taken as in Equation (101), that prescribes a linear shape function for the damage field within the transition layer; the damage evolution law follows from a local dissipation expressed as in (38) where the function $Y_c(d)$ is given by Equation (88), which is in turn obtained based on the equivalence with an intrinsic cohesive law with linear softening.

In numerical applications either structured or unstructured meshes made of quadrilateral elements are used. FE meshes do not need to be uniform to obtain objective results and elements with a characteristic size h ranging from one sixth to one third of the length scale l_c have been found sufficient in all the examined cases to adequately resolve the damage process zone.

All computations have been carried out with a customized version of the finite element code FEAP⁴⁸ using an arc-length control and a termination criterion expressed in terms of the incremental energy norm⁴⁹ as:

$$E^{(i)} \leq \varrho E^{(0)} \quad (117)$$

with a tolerance $\varrho = 10^{-16}$.

7.1 | Problem 1: Imperfect traction bar

As a first example we consider the classical problem of the imperfect bar under tension already analyzed by Geers et al.²⁶ that is shown in Figure 5.

The bar has length $L = 100$ mm and cross section area $A = 10$ mm²; strain localization is triggered with a geometrical imperfection consisting of a cross section area reduction of 10% in the center of the bar over a length of 2.5 mm. Loading is simulated by prescribing nodal forces at the right end of the bar via arc-length control.

Elastic moduli are $E = 2500$ MPa and $\nu = 0$, the peak stress is set as $\sigma_f = 12.5$ MPa, which corresponds to the limit strain $\varepsilon_o = 5.0 \cdot 10^{-3}$ used by Geers et al.,²⁶ while the parameter λ defined by (82) has been taken equal to 1/3 to comply with conditions (73) and (74).

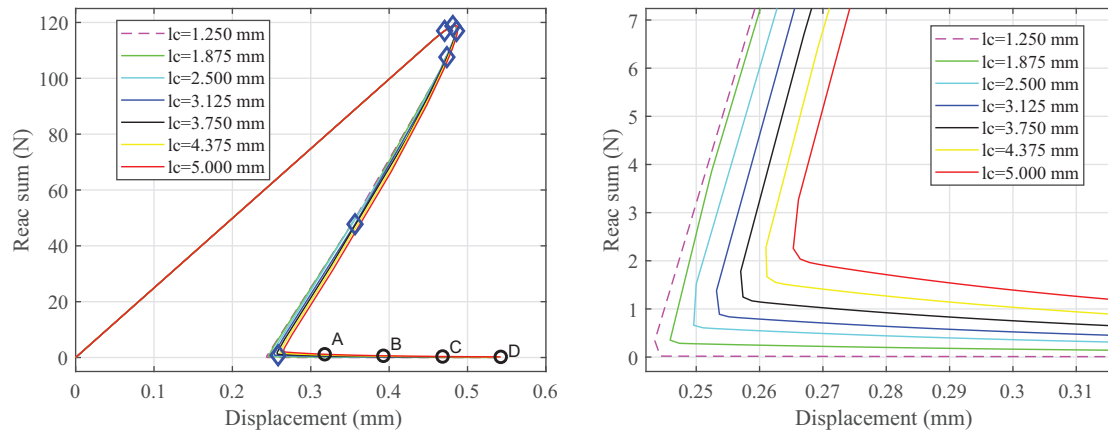


FIGURE 6 Imperfect bar in tension. Load-displacement curves at varying length scale l_c (left) and enlarged view at the end of the localization phase (right)

The problem is solved with seven different values of the length scale l_c using 4-noded elements within a structured nonuniform mesh. For the coarse mesh the element size is 0.625 mm for the 50 mm-wide central part of the bar and 1.25 mm for the remaining part; a refined mesh is also considered with halved element size that yields almost identical results.

Figure 6 depicts the global load-elongation curves obtained at varying l_c between 1.25 and 5.00 mm. These curves exhibit three distinct stages of the structural response, that is: a first part with load and elongation increase corresponding to initial elastic behavior; a second part with a snap-back that corresponds to the strain localization phase; a third part where the bar elongation starts to grow again that is characterized by the occurrence of fracture strains and vanishing material stiffness. As expected, the smaller the length scale parameter l_c , the sharper is the snap-back, see for example, the enlarged view of the load-deflection curves in Figure 6.

Figure 7 depicts damage evolution during the localization phase. The snapshots correspond to the six points highlighted in blue in Figure 6; here it is noted that damage tends to stabilize once the plateau $d = 1$ is reached in the two central weakened elements.

In Figure 8 is depicted the gradient of damage norm, that is, the nonlocal constrained quantity of the model, at the end of the localization phase; the relevant damage distribution corresponds to the last snapshot in Figure 7. The gradient plot in Figure 8 shows that the size of the transition zone between the completely damaged region and the sound material is controlled by the constraint Equation (18), that fixes the length scale parameter l_c and prescribes the shape of the damage distribution.

The gradients in Figure 8 have been postcomputed using finite differences; this figure shows the tendency to a zero gradient of damage in the middle of the bar at complete localization that can also be appreciated in Figure 9, where we report the damage distributions corresponding to points labeled A to D in Figure 6.

Use of Lagrange multipliers is successful to inhibit damage propagation outside the transition band also after the gradient of damage has attained its limiting value. Indeed, Figure 9 clearly shows that upon further loading, that is, further displacement of the bar end, the damage band does not propagate under (almost) zero load even if the strains keep on increasing under zero stress because damage is a constrained field (and not only strain-controlled). This property overcomes one of the main limitations of classical gradient-enhanced continuum damage models, where damage evolution is generally accompanied by spreading of the damaged zone unless a variable damage activity is considered in the diffusion equation that governs damage growth.^{26,28}

In closing this section it is worth emphasizing what follows. In our computations the fracture energy (and by consequence the ductility) increases with the half-width l_c of the localization band, see for example, Figure 6. However, given the size of the structure and the relatively large defect, the geometry considered in the simulation is not well suited for the calibration of material parameters because in an experimental traction test one would experience a catastrophic failure right after the peak load. Actually, for the purpose of parameter calibration one should use a very short tensile specimen (and a stiff testing device) so to make the fracture strains evolve in a stable manner. This would make possible to obtain the complete load-elongation curve, including the softening part. In particular, for the material data set considered in this

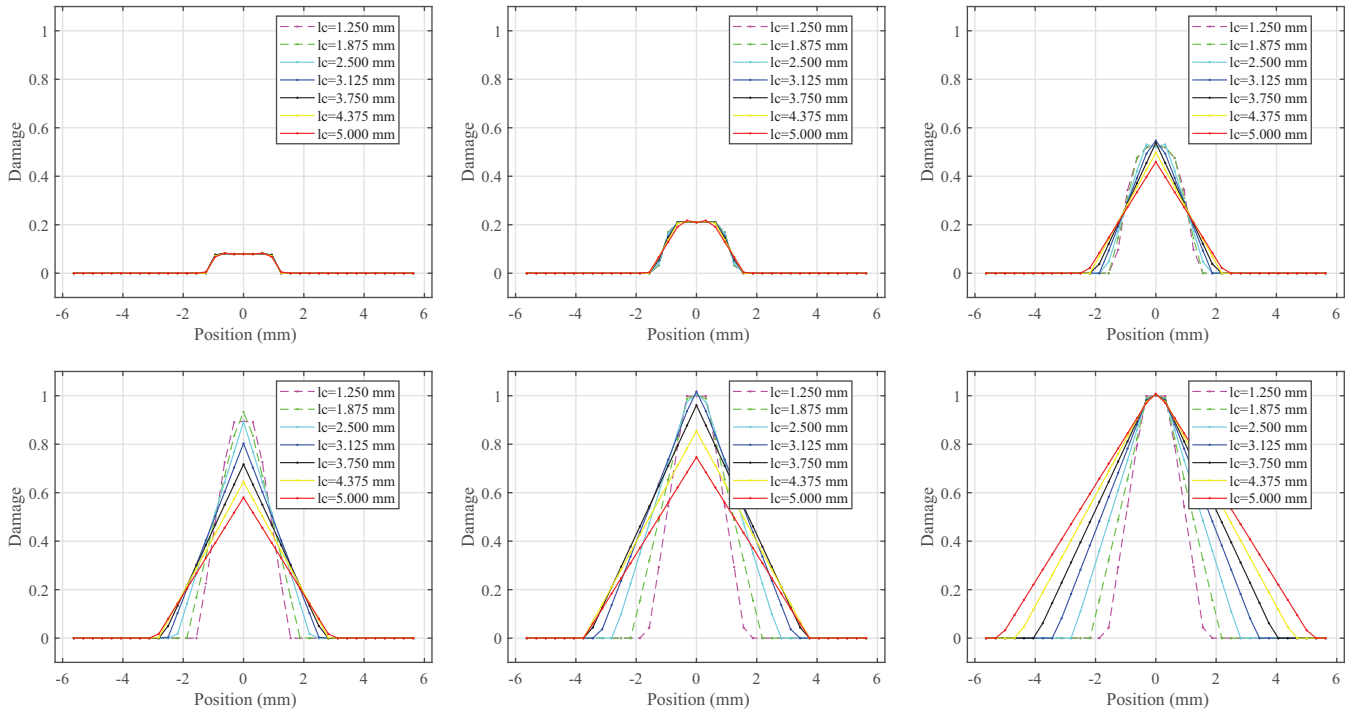


FIGURE 7 Imperfect bar in tension. Damage evolution during the localization phase

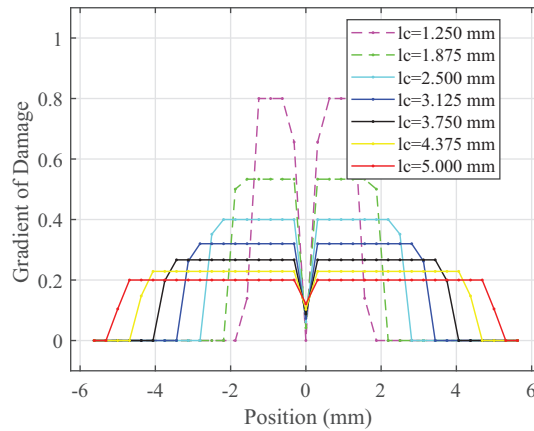


FIGURE 8 Imperfect bar in tension. Gradient of damage distribution at complete localization

example the length of a homogeneous bar for which one would obtain no snap back for all the considered values of l_c should be 7.50 mm.

The tensile bar problem described so far has been analyzed as a two-dimensional problem with a relatively coarse structured mesh. The process zone has been resolved with quite good accuracy and nonbroadening damage behavior during the fracture stage has been always observed, see also Figure 10. This feature is considered to be one of the most remarkable properties of phase-field models; however, such models are mostly suitable for problems with vanishing length scales, whereby in most cases they require extremely refined meshes in order to get converged results.

7.2 | Problem 2: Edge-cracked plate

The following numerical example has been first proposed by Miehe et al.¹³ and is considered to be a numerical proof of the Γ -convergence property for the regularized functional of phase-field models.⁴⁰ It consists of a square plate

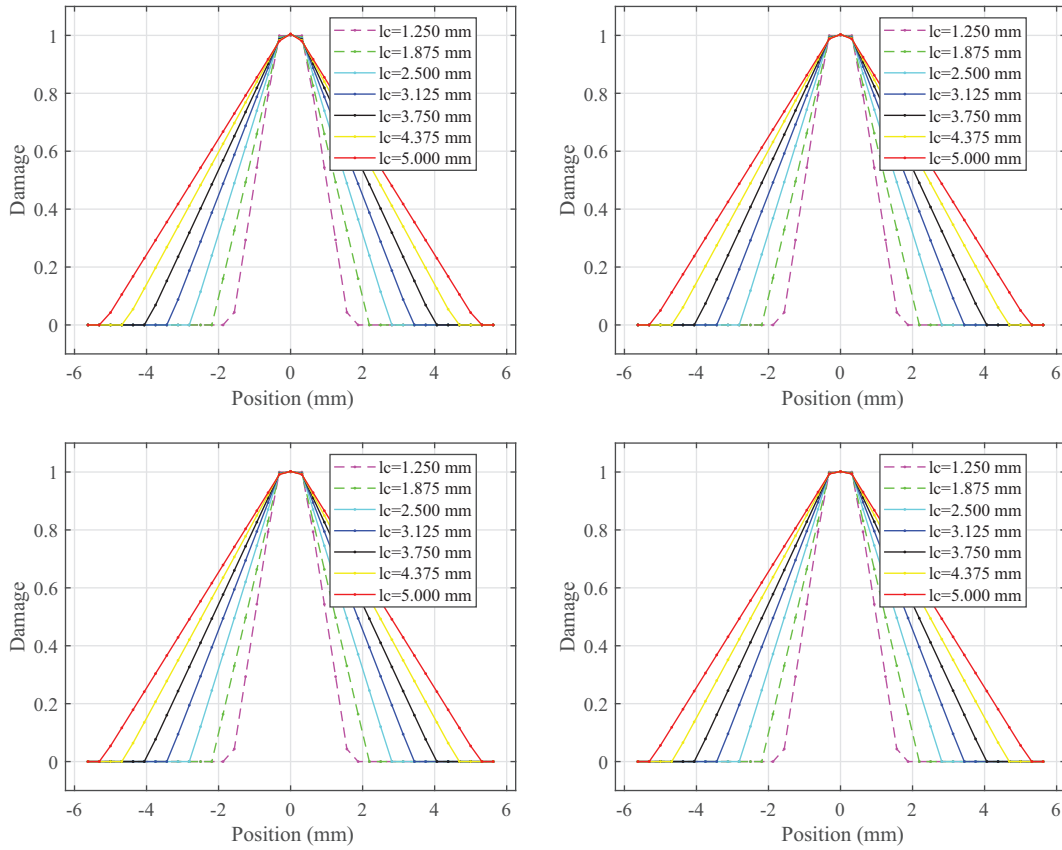


FIGURE 9 Imperfect bar in tension. Damage distribution beyond snap-back (from left to right: points A to D in Figure 6)

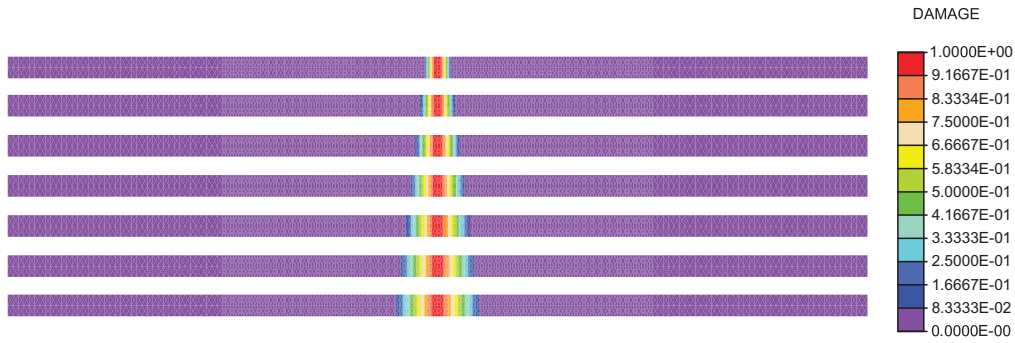


FIGURE 10 Imperfect bar in tension. Damage distribution at final stage of loading process for different length scales l_c (from top to bottom: $l_c = 1.250$ mm, $l_c = 1.875$ mm, $l_c = 2.500$ mm, $l_c = 3.125$ mm, $l_c = 3.750$ mm, $l_c = 4.375$ mm, $l_c = 5.000$ mm)

with sides of unit length and a sharp horizontal crack along a line S from the left edge to the center as shown in Figure 11.

The presence of the crack is simulated via a Dirichlet boundary condition $d = 1$ along S , while on the outer boundary the following boundary condition holds:

$$\gamma_2 \frac{\nabla d}{\|\nabla d\|} \cdot \mathbf{n} = 0. \quad (118)$$

For the case depicted in Figure 11 the above condition is equivalent to prescribe a zero normal derivative of damage on the outer boundary as in classical gradient damage models since the line S is orthogonal to the left edge; however, as shown later on, this is not always the case.

Finite element computations are first carried out with different values of the parameter l_c and a uniform structured mesh of 160×160 linear quadrilaterals (mesh size is $h = 0.00625$ mm). This is a rather coarse mesh compared to the one used to perform the same computations using a phase-field model by Wu,⁴⁰ for which the mesh size has to be extremely small to resolve the length scale. In particular, for this problem a mesh of more than one million elements (1,325,000 linear triangles) has been used, that is considered to be computationally acceptable by the Author since the diffusion problem that governs the evolution of the phase-field is linear.⁴⁰

Figure 12 shows the solutions computed based on the graded damage model at varying length scale l_c . The transition band with linear variation is perfectly captured in all the examined cases even with only two elements per each side of the prescribed crack within the process zone; the homogeneous boundary condition for the normal damage derivative is recognized to hold.

Besides computational efficiency, the greater flexibility of the graded damage formulation compared to classical gradient formulations, that use a zero-normal derivative of damage as natural boundary condition, can be demonstrated via a slightly modified version of the edge-cracked plate shown in Figure 13. As in the original version of the problem, we here prescribe a unit damage value along a straight line S but now the line is no longer orthogonal to the outer boundary. The boundary condition (118) still applies.

Computations are carried out using a fixed length scale $l_c = 0.05$ mm and the nonuniform nonstructured mesh consisting of 4309 linear quadrilaterals depicted in Figure 13 that has been obtained using the mesh generator GMSH.⁵⁰ The computed damage distribution is depicted in Figure 14. Here it is shown that the boundary condition (118) is not equivalent to a zero normal derivative of damage on the outer boundary. Actually, in this case the Lagrange multiplier γ_2 is nihil on the outer boundary because here the gradient of damage does not meet the condition $g_2(d) \leq 0$.

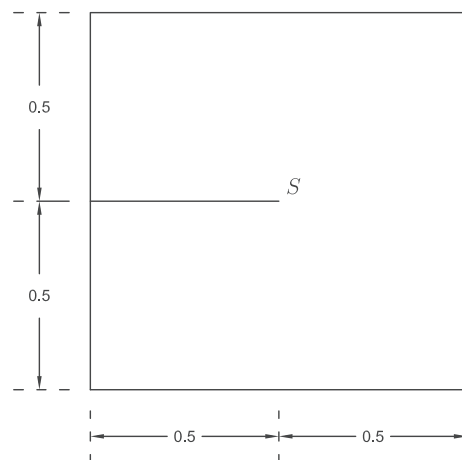


FIGURE 11 Edge-cracked plate. Model problem

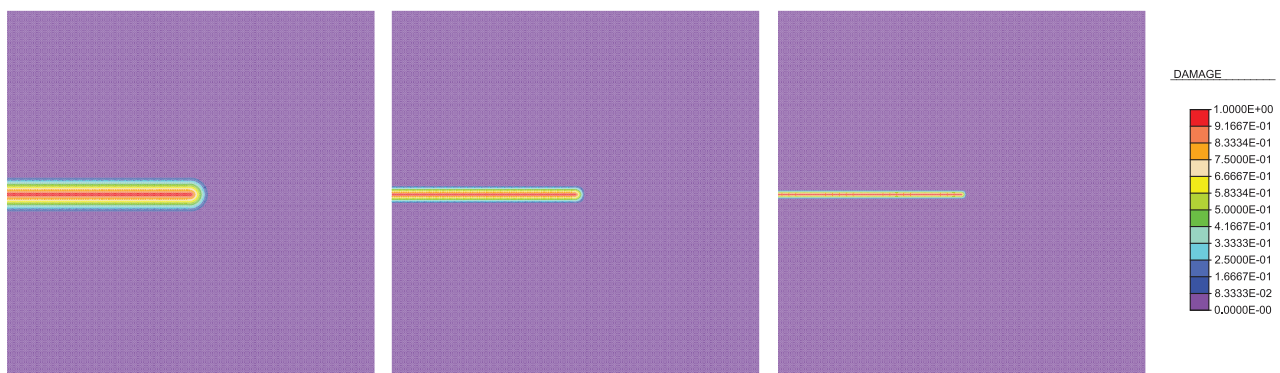


FIGURE 12 Edge-cracked plate. Damage distribution for different length scales l_c (from left to right: $l_c = 0.05$ mm, $l_c = 0.025$ mm, $l_c = 0.0125$ mm). The thickness of the damaged region equals $2l_c$

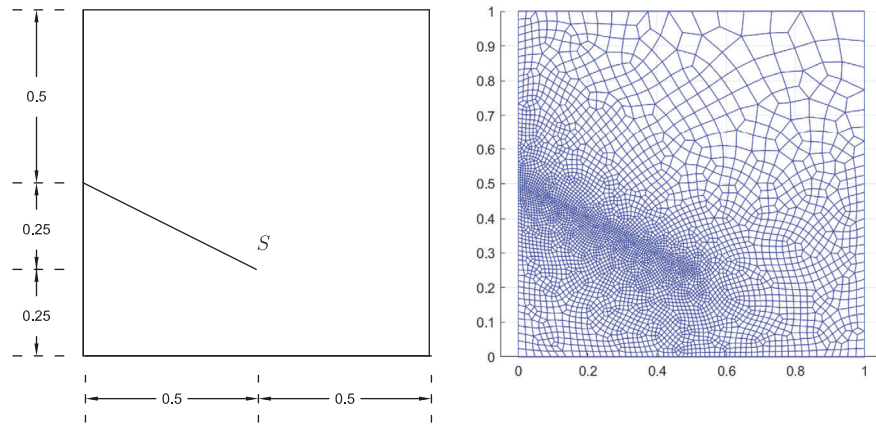


FIGURE 13 Modified edge-cracked plate. Model problem and FE mesh

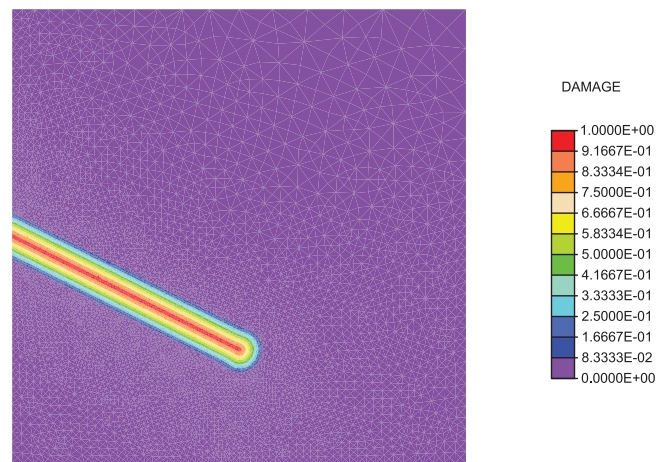


FIGURE 14 Modified edge-cracked plate. Damage distribution ($l_c = 0.05$ mm)

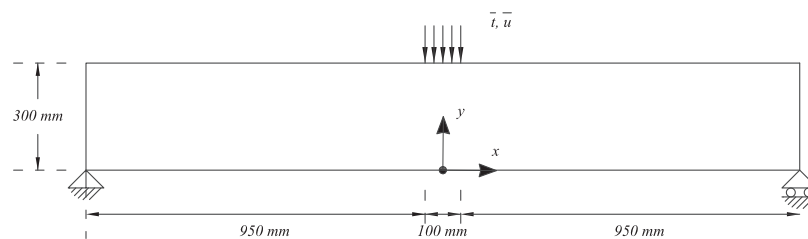


FIGURE 15 Three-point bending of a beam. Model problem

7.3 | Problem 3: Three-point bending of a beam

Next we consider the unnotched beam under three-point bending shown in Figure 15.^{27,51} This example is used by De Borst and Verhoosel²⁷ to show the spreading of the damaged region during crack propagation; this is a well-known artifact of classical strain-based gradient damage formulations with constant diffusion, whereby such models are considered not suitable to reproduce very brittle responses, that often correspond to situations with narrow localization bands or sharp cracks.

The beam has length $2L = 2000$ mm, height $h = 300$ mm, thickness $b = 50$ mm and is analyzed under plane strain conditions. Displacement boundary conditions consist of two point supports while loading is prescribed by a uniform

tractions distribution over a 100 mm-wide region in the center of the beam, see also Figure 15. Following De Borst and Verhoosel²⁷ the elastic moduli are taken as $E = 20 \text{ GPa}$, $\nu = 0.2$, and the peak stress of the equivalent cohesive law is set as $\sigma_f = 2.0 \text{ MPa}$ (the corresponding limit strain is $\varepsilon_0 = 1.0 \cdot 10^{-4}$). Moreover, the parameter l_c has been fixed at 40 mm whereas λ has been taken equal to 0.4, which corresponds to a surface fracture energy $G_f = 2.0 \cdot 10^{-2} \text{ N/mm}$ and a length scale of the cohesive law of 100 mm.

The previous values of the material parameters are consistent with those of a plain concrete. Actually, in our model the length scale l_c represents the half-thickness of the active damage process zone that, in quasi-brittle materials, typically depends on the size of material heterogeneities. As a rough guideline, in concrete-like materials one can take for l_c twice the maximum aggregate size⁵² whereas the nondimensional parameter λ should be chosen in a way to comply with the conditions of local stability (73) and strain softening (74), see also Section 5. The two length scales represented by l_c and λ are responsible for the size effect.

The structure has been modeled using structured meshes of linear quadrilaterals; the coarse mesh consists of 5376 elements and the fine mesh has 11,100 elements. In order to accurately resolve the transition band a mesh refinement is used in the central part of the beam to get a node spacing in both directions of 6.25 mm for the coarse mesh and 4.0 mm for the refined mesh in the 200 mm-wide region located in the middle of the beam; in the 750 mm-wide outermost parts the horizontal node spacing is 25 mm for the coarse mesh and 20.83 mm for the refined mesh while in the intermediate zones (150 mm-wide) horizontal spacing is 12.5 mm for the coarse mesh and 9.375 mm for the refined mesh.

The specimen size, the material data set and the absence of an initial notch in the beam suggest that a quite brittle behavior should be expected; this conjecture is also corroborated by the various brittleness numbers that can be found in the literature,¹ and will be confirmed by numerics. Motivated by these considerations, numerical simulations have been carried out using a CMOD as a constraint for the arc-length control instead of the vertical displacement of the top center of the beam.²⁷ The load-deflection responses are depicted in Figure 16; the curves refer to the two meshes while the highlighted point (F, δ) corresponds to the initial elastic limit that is computed based on Euler–Bernoulli beam theory as:

$$F = \sigma_f \frac{b h^2}{3 L}; \quad \delta = \frac{\sigma_f}{E} \frac{2 L^2}{3 h}. \quad (119)$$

As expected, the numerically computed load-deflections curves for the coarse and fine mesh reported in Figure 16 exhibit a sharp snap-back and are in substantial agreement. The effect of mesh size is clearly visible in that the mesh refinement allows to correct the bumps present on the propagation branch of the curve pertaining to the coarse mesh.

Except for the initial linear part, these curves cannot be directly compared with those presented by De Borst and Verhoosel²⁷ due to the different damage law; however, a comparison of results can be made in terms of damage iso-value maps, that allow to demonstrate some distinctive features of the graded damage model.

Figure 17 depicts the damage contours for the case $l_c = 40.0 \text{ mm}$ that illustrates damage evolution for the problem at hand. Since no initial defect or notch is present, growth of the damage front naturally starts in the middle of the beam

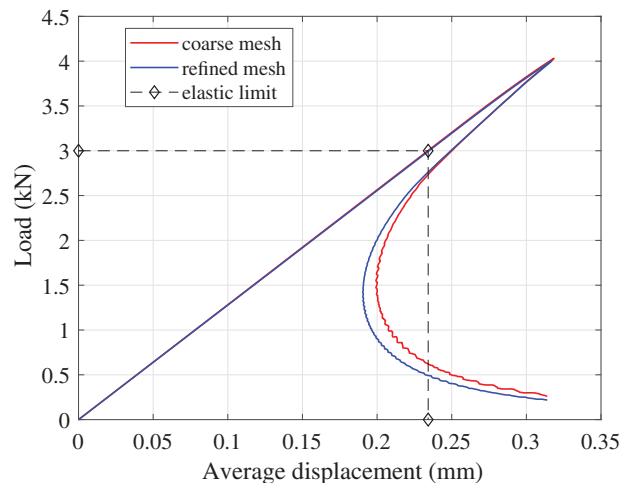


FIGURE 16 Three-point bending of a beam. Load-deflection curves ($l_c = 40 \text{ mm}$)

where the local damage energy release rate Y first attains the initial threshold value; once the transition zone has fully established, that is, the half-width of the interphase equals the length scale l_c , the crack starts to propagate in a self-similar way and the front advances.

On the contrary, results presented in the literature, see for example, figure 13 in the article of Askes et al.⁵¹ or figure 4 in the article of De Borst and Verhoosel,²⁷ show that the damage distribution during crack propagation is accompanied by a significant damage spread on the bottom of the beam as a consequence of the continuous growth of the averaged strain measure in the vicinity of the crack. This last feature, that is in a sense intrinsic to the classical implicit gradient models, is strongly related to the diffusion equation with a constant strain activity parameter that governs damage evolution and to the homogeneous Neumann boundary condition that is universally adopted in classical gradient models.

The iso-damage maps presented in Figure 17 refer to the coarse mesh; use of the refined mesh does not affect these maps that remain practically identical. Damage evolution exhibits exactly the same features when the length scale is increased by a factor 2. This fact can be appreciated in Figure 18, where the sequence of iso-damage contours obtained for the case $l_c = 80$ mm shows that the nonlocal constraint (18) acting on the damage field plays the role of an optimal diffusion limiter in that it inhibits nonphysical damage spread. A three-point bending problem almost identical to the one discussed so far has been solved by Bernard et al.⁵³ using the TLS approach. In particular, the smoother damage profiles computed therein using a mesh consisting of 34,478 quadratic triangles do compare pretty well with those reported in Figures 17 and 18 though the load-deflection curves are not coincident because of the different data set.

7.4 | Problem 4: Interacting cracks in a double-notched plate

As a last example we study a nonsymmetric double edge notched specimen under tensile load. This is a well-known test that is used to investigate the ability of damage and fracture models to reproduce curved cracks interacting each other during growth.^{54,55}

Figure 19 shows the geometry and the boundary conditions of the structure that is analyzed under plane strain conditions. Loading is applied by prescribing vertical displacements \bar{u} on the upper edge of the plate^{33,56} and material parameters are taken as $E = 210$ kN/mm², $\nu = 0.3$, critical fracture energy $G_f = 2.7 \cdot 10^{-3}$ kN/mm. The main length scale parameter governing the width of the localization band is taken as $l_c = 1$ mm while the parameter λ has been chosen equal to 0.4, which corresponds to a length scale of the equivalent cohesive law of 2.5 mm and a peak stress $\sigma_f = 4.76$ kN/mm².

The structure is discretized using the unstructured mesh shown in Figure 19 consisting of 9189 quadrilateral elements that is conveniently refined in the region where crack propagation is expected; the obtained minimum element size $h =$

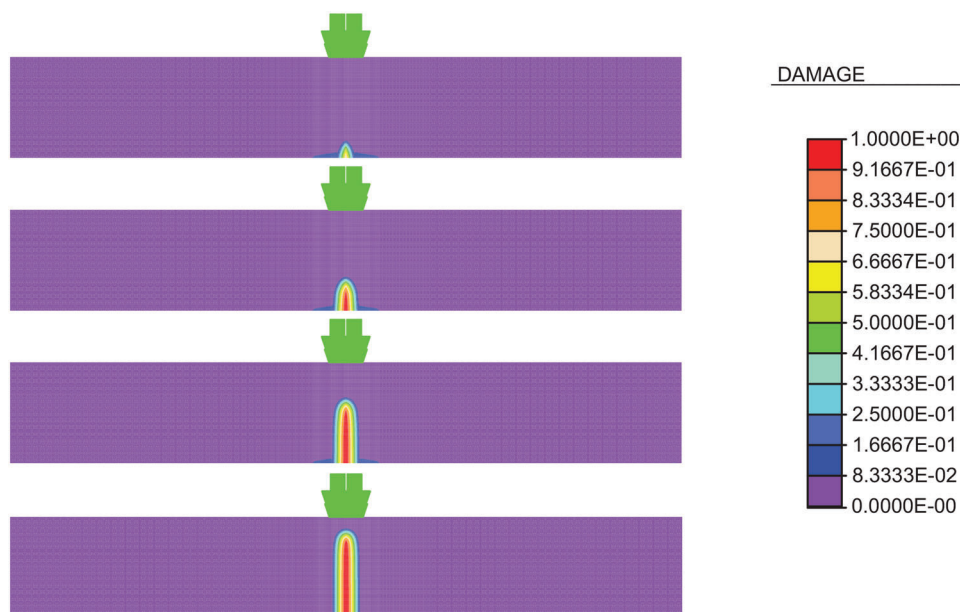


FIGURE 17 Three-point bending of a beam. Iso-damage maps showing damage evolution for $l_c = 40.0$ mm

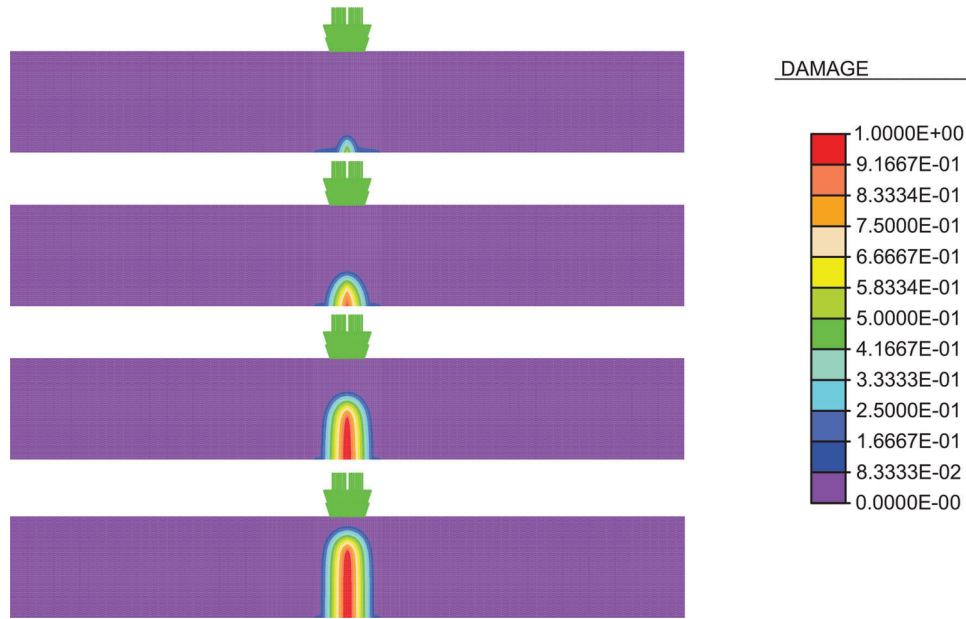


FIGURE 18 Three-point bending of a beam. Iso-damage maps showing damage evolution for $l_c = 80.0$ mm

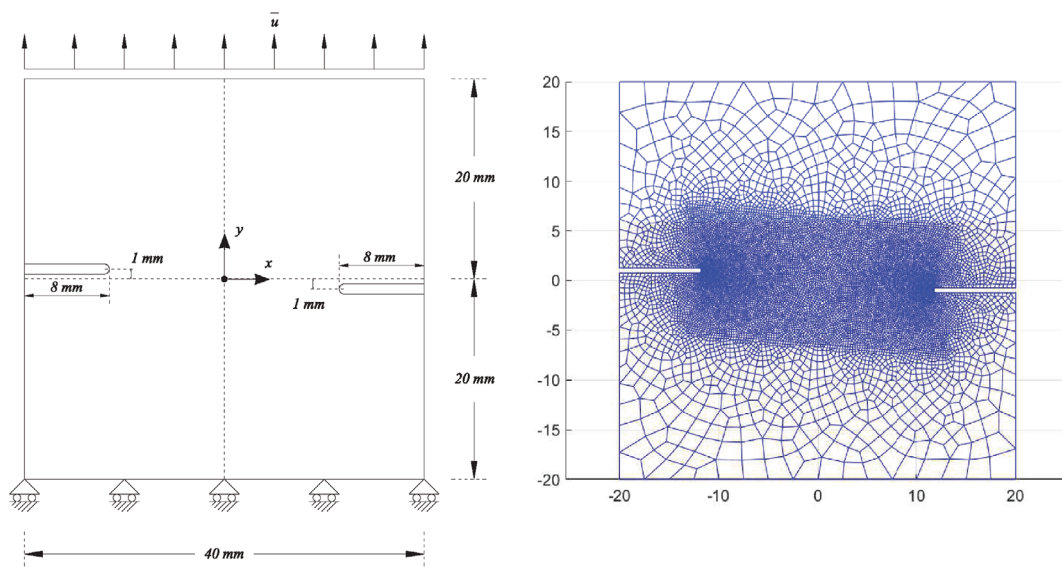


FIGURE 19 Asymmetric double-notched plate. Model problem and FE mesh

0.1 mm is able to resolve the transition band between the sound material and the damaged one. This is a quite coarse mesh compared to the one used by Nguyen et al.³³ that contains about 50,000 elements (but using an internal length scale of 0.135 mm).

Figure 20 depicts the load-deflection curve that has been obtained using $\Delta \bar{u} = 1 \mu\text{m}$ for the first 30 steps followed by increments reduced to $0.1 \mu\text{m}$. The results in terms of crack evolution are summarized in Figure 21; here are reported the contour plots of the damage iso-values corresponding to points labeled *A* to *D* in Figure 20. A good qualitative correspondence is found with the behavior described in the article of Sumi and Wang,⁵⁵ that is, that during propagation the two cracks first rotate away from one another, then turn in the opposite direction and finally coalesce.

In closing this section we emphasize that all the information necessary to track the evolution of interphases in a state of progressive damage is implicitly contained in the Lagrange multiplier field associated to the constraint acting on the gradient of damage. Though implicitly, the Lagrange multipliers replace distance functions and all difficulties emanating

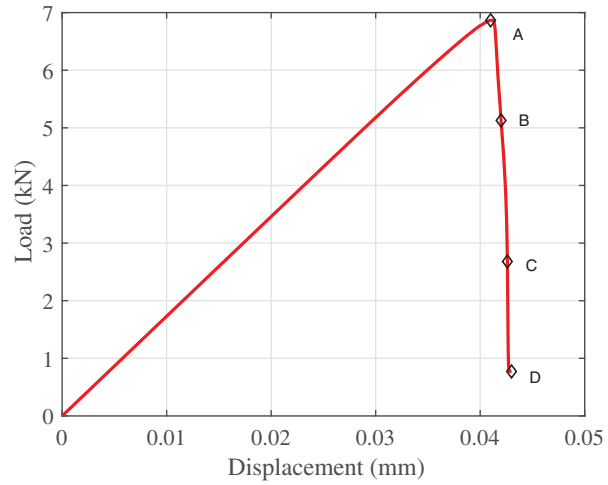


FIGURE 20 Asymmetric double-notched plate. Load-deflection curve

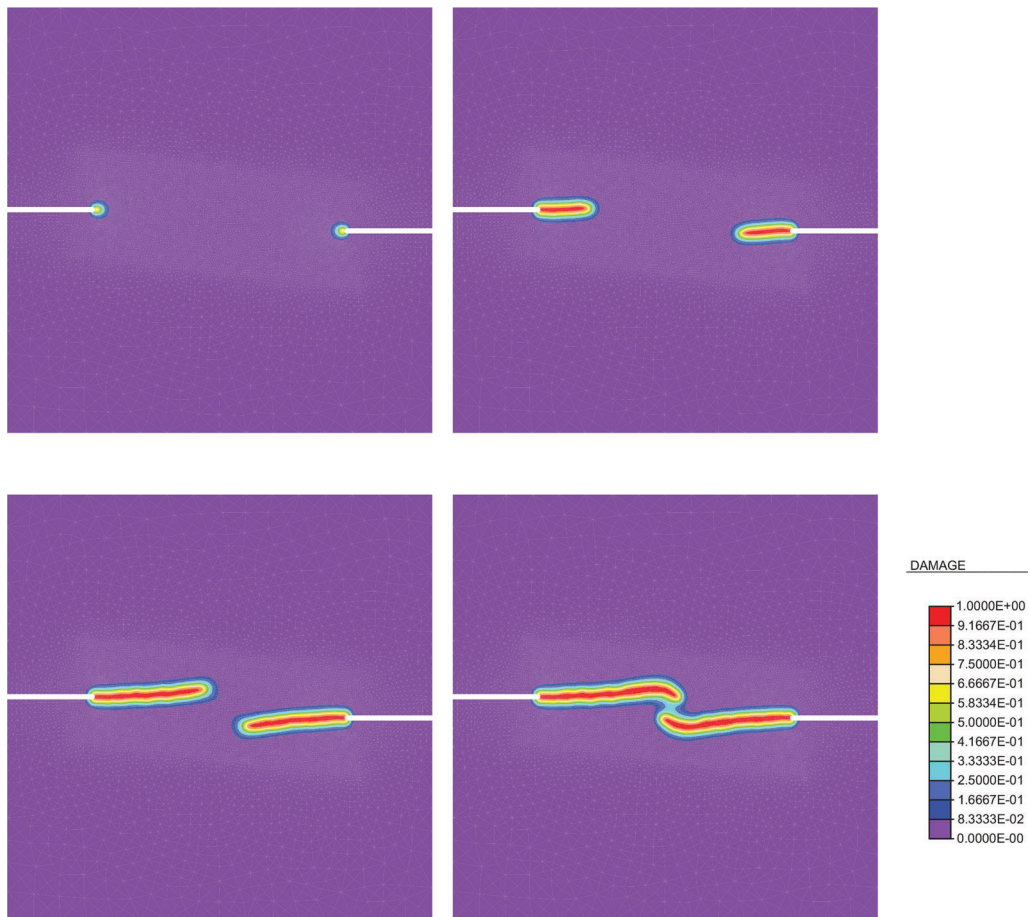


FIGURE 21 Asymmetric double-notched plate. Snapshots of crack growth (points A to D in Figure 20)

from the implementation of level sets into a Finite Element code, whereby the problem is recast in the more classical framework of nonsmooth generalized standard models of evolutionary type.

8 | SUMMARY AND CONCLUSIONS

We presented a new gradient-based damage formulation, the *graded damage model*, that has much in common, but also some distinctive features, compared to the moving thick layer approach that is known in the literature in the form of the *thick level set* (TLS) model. Unlike its more famous relative, in the present formulation the introduction of level sets with all consequent difficulties is abandoned and the information necessary to track the evolution of interphases where progressive damage occurs is transferred into two Lagrange multipliers fields acting on constraint equations that are expressed in terms of convex functions.

Among the notable features of the graded damage model is the fact that it naturally fits in the generalized standard setting, for which a normality rule holds. Moreover, the internal constraints being nondissipative, the only dissipation comes from the local damage energy release rate. From the numerical standpoint, the incremental update of the state of the system is carried out via a staggered computational scheme for a Lagrange multiplier problem; this is in turn obtained based on the nondissipative character of the constraints that allows to set up a three-field functional to render stationary with respect to the arguments.

The variational structure of the problem, to which relaxed Neumann boundary conditions on the damage field apply, allow for an effective implementation, and the applications documented in the article have demonstrated the ability to perform Finite Element computations. In particular, localization bands are well captured both for structured and unstructured meshes, no spurious spreading of damaged regions is observed during crack propagation and all computations are successfully terminated with quite coarse meshes compared to classical gradient-damage and phase-field formulations.

The model presented in this article is amenable to a number of extensions and further work is needed to implement the necessary enhancements needed to handle more complex situations, for example, three-dimensional problems among others, and extensively compare with experimental data from concrete literature. These topics are still the object of ongoing research and will be dealt with in forthcoming article.

CONFLICT OF INTEREST

The authors declare no potential conflict of interests.

ORCID

Nunziante Valoroso  <https://orcid.org/0000-0001-8830-1964>

REFERENCES

1. Bažant Z, Planas J. *Fracture and Size Effect in Concrete and Other Quasibrittle Materials*. CRC Press; 1998.
2. Pijaudier-Cabot G, Bažant Z. Nonlocal damage theory. *J Eng Mech*. 1987;113(10):1512-1533. doi:10.1061/(ASCE)0733-9399(1987)113:10(1512)
3. Peerlings R, De Borst R, Brekelmans W, De Vree J. Gradient enhanced damage for quasi-brittle materials. *Int J Numer Methods Eng*. 1996;39(19):3391-3403. doi:10.1002/(SICI)1097-0207(19961015)39:19<3391::AID-NME7>3.0.CO;2-D
4. Peerlings R, De Borst R, Brekelmans W, De Vree J, Spee I. Some observations on localization in non-local and gradient damage models. *Eur J Mech A/Solids*. 1996;15(6):937-953.
5. Frémond M, Nedjar B. Damage, gradient of damage and principle of virtual power. *Int J Solids Struct*. 1996;33(8):1083-1103. doi:10.1016/0020-7683(95)00074-7
6. Aifantis E. On the microstructural origin of certain inelastic models. *J Eng Mater Technol*. 1984;106(4):326-330. doi:10.1115/1.3225725
7. Lasry D, Belytschko T. Localization limiters in transient problems. *Int J Solids Struct*. 1988;24(6):581-597. doi:10.1016/0020-7683(88)90059-5
8. De Borst R, Mühlhaus HB. Gradient-dependent plasticity: formulation and algorithmic aspects. *Int J Numer Methods Eng*. 1992;35(3):521-539. doi:10.1002/nme.1620350307
9. Fleck N, Hutchinson J. A phenomenological theory for strain gradient effects in plasticity. *J Mech Phys Solids*. 1993;41(12):1825-1857. doi:10.1016/0022-5096(93)90072-N
10. Peerlings R, Geers M, De Borst R, Brekelmans W. A critical comparison of nonlocal and gradient-enhanced softening continua. *Int J Solids Struct*. 2001;38(44-45):7723-7746. doi:10.1016/S0020-7683(01)00087-7
11. Francfort G, Marigo JJ. Revisiting brittle fracture as an energy minimization problem. *J Mech Phys Solids*. 1998;46(8):1319-1342. doi:10.1016/S0022-5096(98)00034-9

12. Bourdin B, Francfort G, Marigo JJ. Numerical experiments in revisited brittle fracture. *J Mech Phys Solids*. 2000;48(4):797-826. doi:10.1016/S0022-5096(99)00028-9
13. Miehe C, Welschinger F, Hofacker M. Thermodynamically consistent phase-field models of fracture: variational principles and multi-field FE implementations. *Int J Numer Methods Eng*. 2010;83(10):1273-1311. doi:10.1002/nme.2861
14. Miehe C, Hofacker M, Welschinger F. A phase field model for rate-independent crack propagation: robust algorithmic implementation based on operator splits. *Comput Methods Appl Mech Eng*. 2010;199(45):2765-2778. doi:10.1016/j.cma.2010.04.011
15. Ambrosio L, Tortorelli V. Approximation of functional depending on jumps by elliptic functional via Γ -convergence. *Commun Pure Appl Math*. 1990;43(8):999-1036. doi:10.1002/cpa.3160430805
16. Mumford D, Shah J. Optimal approximations by piecewise smooth functions and associated variational problems. *Commun Pure Appl Math*. 1989;42(5):577-685. doi:10.1002/cpa.3160420503
17. Freddi F, Royer-Carfagni G. Regularized variational theories of fracture: a unified approach. *J Mech Phys Solids*. 2010;58(8):1154-1174. doi:10.1016/j.jmps.2010.02.010
18. Lorentz E, Godard V. Gradient damage models: toward full-scale computations. *Comput Methods Appl Mech Eng*. 2011;200(21-22):1927-1944. doi:10.1016/j.cma.2010.06.025
19. Lorentz E, Andrieux S. A variational formulation for nonlocal damage models. *Int J Plast*. 1999;15(2):119-138. doi:10.1016/S0749-6419(98)00057-6
20. Lorentz E, Benallal A. Gradient constitutive relations: numerical aspects and application to gradient damage. *Comput Methods Appl Mech Eng*. 2005;194(50-52):5191-5220. doi:10.1016/j.cma.2004.12.016
21. Halphen B, Nguyen QS. Sur les Matériaux Standard Généralisés. *J de Méc*. 1975;14:39-63.
22. Ponter A, Bataille J, Kestin J. A thermodynamic model for the time dependent plastic deformation of solids. *J de Méc*. 1979;18:511-539.
23. Comi C. Computational modelling of gradient-enhanced damage in quasi-brittle materials. *Mech Cohesive-frict Mater*. 1999;4(1):17-36. doi:10.1002/(SICI)1099-1484(199901)4:1<17::AID-CFM55>3.0.CO;2-6
24. Lorentz E, Cuvilliez S, Kazymyrenko K. Convergence of a gradient damage model toward a cohesive zone model. *Comptes Rendus Mécanique*. 2011;339(1):20-26. doi:10.1016/j.crme.2010.10.010
25. Alfano G, Rosati L, Valoroso N. A displacement-like finite element model for J2 elastoplasticity: variational formulation and finite-step solution. *Comput Methods Appl Mech Eng*. 1998;155(3-4):325-358. doi:10.1016/S0045-7825(97)00171-0
26. Geers M, De Borst R, Brekelmans W, Peerlings R. Strain-based transient-gradient damage model for failure analyses. *Comput Methods Appl Mech Eng*. 1998;160(1-2):133-153. doi:10.1016/S0045-7825(98)80011-X
27. De Borst R, Verhoosel C. Gradient damage vs phase-field approaches for fracture: similarities and differences. *Comput Methods Appl Mech Eng*. 2016;312:78-94. doi:10.1016/j.cma.2016.05.015
28. Saroukhani S, Vafadari R, Simone A. A simplified implementation of a gradient-enhanced damage model with transient length scale effects. *Comput Mech*. 2013;51:899-909. doi:10.1007/s00466-012-0769-8
29. Poh LH, Sun G. Localizing gradient damage model with decreasing interactions. *Int J Numer Methods Eng*. 2017;110(6):503-522. doi:10.1002/nme.5364
30. Simone A, Askes H, Peerlings R, Sluys L. Interpolation requirements for implicit gradient-enhanced continuum damage models. *Commun Numer Methods Eng*. 2004;20(2):163-165. doi:10.1002/cnm.663
31. Nguyen QS, Andrieux S. The non-local generalized standard approach: a consistent gradient theory. *Comptes Rendus Mécanique*. 2005;333(2):139-145. doi:10.1016/j.crme.2004.09.010
32. Moës N, Stolz C, Bernard PE, Chevaugeon N. A level set based model for damage growth: the thick level set approach. *Int J Numer Methods Eng*. 2011;86(3):358-380. doi:10.1002/nme.3069
33. Nguyen TT, Yvonnet J, Waldmann D, He QC. Implementation of a new strain split to model unilateral contact within the phase field method. *Int J Numer Methods Eng*. 2020;121(21):4717-4733. doi:10.1002/nme.6463
34. Coleman B, Gurtin M. Thermodynamics with internal state variables. *J Chem Phys*. 1967;47(2):597-613. doi:10.1063/1.1711937
35. Frémond M, Stolz C. On alternative approaches for graded damage modelling. In: Frémond M, Maceri F, Vairo G, eds. *Models, Simulation, and Experimental Issues in Structural Mechanics*. Springer Series in Solid and Structural Mechanics. Springer; 2017.
36. Rastello G, Giry C, Gatuingt F, Desmorat R. From diffuse damage to strain localization from an Eikonal Non-Local (ENL) Continuum Damage model with evolving internal length. *Comput Methods Appl Mech Eng*. 2018;331:650-674. doi:10.1016/j.cma.2017.12.006
37. Germain P, Nguyen Q, Suquet P. Continuum thermodynamics. *J Appl Mech*. 1983;50(4b):1010-1020. doi:10.1115/1.3167184
38. Stolz C. On moving thick layer approach for graded damage modelling. *Int J Fract*. 2016;202:195-205. doi:10.1007/s10704-016-0154-2
39. Parrilla Gómez A, Moes N, Stolz C. Comparison between thick level set (TLS) and cohesive zone models. *Adv Model Simul Eng Sci*. 2015;2:2-18. doi:10.1186/s40323-015-0041-9
40. Wu JY. A unified phase-field theory for the mechanics of damage and quasi-brittle failure. *J Mech Phys Solids*. 2017;103:72-99. doi:10.1016/j.jmps.2017.03.015
41. Lorentz E, Cuvilliez S, Kazymyrenko K. Modelling large crack propagation: from gradient damage to cohesive zone models. *Int J Fract*. 2012;178:85-95. doi:10.1007/s10704-012-9746-7
42. Lemaitre J, Chaboche J. *Mécanique des Matériaux Solides*. Dunod; 1985 English translation: *Mechanics of Solid Materials*, Cambridge University Press, Cambridge, 1990.
43. Bertsekas D. *Convex Optimization Algorithms*. 1st ed. Athena Scientific; 2015.
44. Parrilla Gómez A, Stolz C, Moës N, Grégoire D, Pijaudier-Cabot G. On the capability of the Thick Level Set (TLS) damage model to fit experimental data of size and shape effects. *Eng Fract Mech*. 2017;184:75-87. doi:10.1016/j.engfracmech.2017.07.014

45. Wheeler M, Wick T, Wollner W. An augmented-Lagrangian method for the phase-field approach for pressurized fractures. *Comput Methods Appl Mech Eng*. 2014;271:69-85. doi:10.1016/j.cma.2013.12.005
46. Bertsekas D. *Constrained Optimization and Lagrange Multiplier Methods*. Athena Scientific Series in Optimization and Neural Computation Massachusetts. 1st ed. Athena Scientific; 1996.
47. Rosati L, Valoroso N. A return map algorithm for general isotropic elasto/visco-plastic materials in principal space. *Int J Numer Methods Eng*. 2004;60(2):461-498. doi:10.1002/nme.970
48. Taylor RL. *FEAP - Programmer Manual*. University of California; 2021 <http://www.ce.berkeley.edu/projects/feap/>.
49. Zienkiewicz OC, Taylor RL. *The Finite Element Method, Vol. II: Solid Mechanics*. Butterworth-Heinemann; 2000.
50. Geuzaine C, Remacle J. Gmsh: a 3-D finite element mesh generator with built-in pre- and post-processing facilities. *Int J Numer Methods Eng*. 2009;79(11):1309-1331. doi:10.1002/nme.2579
51. Askes H, Pamin J, De Borst R. Dispersion analysis and element-free Galerkin solutions of second- and fourth-order gradient-enhanced damage models. *Int J Numer Methods Eng*. 2000;49(6):811-832. doi:10.1002/1097-0207(20001030)49:6<811::AID-NME985>3.0.CO;2-9
52. Grégoire D, Rojas-Solano L, Pijaudier-Cabot G. Failure and size effect for notched and unnotched concrete beams. *Int J Numer Anal Methods Geomech*. 2013;37(10):1434-1452. doi:10.1002/nag.2180
53. Bernard P, Moës N, Chevaugeon N. Damage growth modeling using the Thick Level Set (TLS) approach: efficient discretization for quasi-static loadings. *Comput Methods Appl Mech Eng*. 2012;233-236:11-27. doi:10.1016/j.cma.2012.02.020
54. Melin S. Why do cracks avoid each other? *Int J Fract*. 1983;23(1):37-45. doi:10.1007/BF00020156
55. Sumi Y, Wang Z. A finite-element simulation method for a system of growing cracks in a heterogeneous material. *Mech Mater*. 1998;28(1):197-206. doi:10.1016/S0167-6636(97)00048-3
56. Nguyen K, Augarde C, Coombs W, Nguyen-Xuan H, Abdel-Wahab M. Non-conforming multipatches for NURBS-based finite element analysis of higher-order phase-field models for brittle fracture. *Eng Fract Mech*. 2020;235:107133. doi:10.1016/j.engfracmech.2020.107133

How to cite this article: Valoroso N, Stolz C. Graded damage in quasi-brittle solids. *Int J Numer Methods Eng*. 2022;1-32. doi: 10.1002/nme.6947